Marine and Petroleum Geology 148 (2023) 106063

Contents lists available at ScienceDirect

Marine and Petroleum Geology

journal homepage: www.elsevier.com/locate/marpetgeo

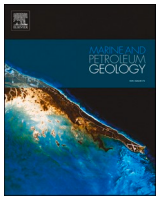

Calculating the large leakage flux of a breached hydrocarbon trap using geophysical interpretation of a paleo-gas-water contact

Benedict L. Campbell *, Martino Foschi, Joseph A. Cartwright

Department of Earth Sciences, University of Oxford, South Parks Road, OX1 3AN, UK

ARTICLE INFO

Keywords:
Top seal breach
Hydrocarbon leakage
Fluid flow
Leakage phenomena
Dynamic gas-water contact
Paleo-gas-water contact
Northern carnarvon basin
North West Shelf of Australia

ABSTRACT

Integration of three-dimensional seismic and well data from the Northern Carnarvon Basin on the North West Shelf of Australia was used to assess the evidence for top seal breach of a paleo-gas accumulation. Several seismic indicators of vertical hydrocarbon leakage from the crest of the stratigraphic Mungaroo Trap point to a significant flux of gas within the past few hundred thousand years. Mapping of the top reservoir within the Triassic aged Mungaroo Formation revealed strong evidence for a paleo-gas-water contact (GWC), approximately 100 m down flank from the erosional crest of the trap. This contact conforms to structure and delimits an original volume of 1.1 trillion cubic feet (Tcf), based on reservoir property calibration from nearby wells. Mapping also revealed a present-day gas-water contact with a closed volume of 0.2 Tcf, 30 m down flank from the crest. This contact displays a discordant geometry indicative of a dynamic contact.

The leakage zone is located directly above the crest of the structure. It is seismically well imaged and comprises seafloor pockmarks, shallow gas anomalies and gas hydrate anomalies. The presence of a leakage zone distributed vertically above a reservoir containing a present and paleo-GWC provides compelling evidence this trap has leaked by breaching of the top seal. Volumetric calculations using the two GWCs indicate that the Mungaroo Trap has been depleted by 0.9–1.1 Tcf. A dynamic-GWC indicates the leakage event within the trap has occurred recently. Analysis of dating of horizons correlated to the seafloor pockmarks places the leakage event at sometime within the last 300 Ka.

1. Introduction

Leakage of hydrocarbons resulting from top seal failure has been documented across a range of petroleum systems (Cowley and O'Brien, 2000; Cox et al., 2021; Fischer et al., 2013; Roberts and Carney, 1997). Leakage by breaching of top seals accounts for a significant fraction of dry holes in hydrocarbon exploration (Downey, 1984; Rudolph and Goulding, 2017). Top seal analysis is therefore an import step in de-risking hydrocarbon prospects (Heggland, 2005; Ingram and Urai, 1999) and is an increasingly important methodological component in appraising potential sites for subsurface carbon sequestration (Chiaramonte et al., 2008; Rahman et al., 2022).

Hydrocarbon leakage has been observed with seismic data, geochemical sampling of surface sediments, direct observation of seepage at the seafloor and bathymetric surveying (Abrams, 1992; Løseth et al., 2009; Rollet et al., 2006). Evidence of hydrocarbon leakage can manifest at the seafloor as pockmark craters, cold seeps or authigenic carbonates (Hovland and Judd, 1988; Kennicutt et al., 1985) and in the subsurface as individual (Heggland, 1997; Sheriff, 1975), or vertically stacked (Berndt et al., 2012; Foschi et al., 2014; Schroot and Schüttenhelm, 2003; Traynor and Sladen, 1997) amplitude anomalies, pipes, seismic chimneys and sediment remobilization structures (Cathles et al., 2010; Gay et al., 2012; Hustoft et al., 2007; Ligtenberg, 2005).

Despite an increased awareness in the diversity of leakage phenomena observable with seismic data, the magnitude of leakage flux required for these phenomena to form is poorly understood. If the leakage flux is not well constrained, it is impossible to know if these 'seismic leakage indicators' are evidence of a blown trap where recoverable commercial reserves have leaked (Hermanrud and Bolås, 2002; Mathieu, 2018; Rudolph and Goulding, 2017) or may instead be evidence that a working petroleum system is present thus providing an indication of deeper prospective reservoirs (Heggland, 1998; Milkov and Samis, 2020).

Previous studies have proposed qualitative assessments of high and low flux seismic leakage phenomena (Heggland, 2005; Roberts and Carney, 1997) and modelling has been used to predict the rate of flux in

* Corresponding author.
E-mail address: benedict.campbell@jesus.ox.ac.uk (B.L. Campbell).

https://doi.org/10.1016/j.marpetgeo.2022.106063
Received 29 April 2022; Received in revised form 5 December 2022; Accepted 6 December 2022
Available online 7 December 2022

vents and gas chimneys (Räss et al., 2018; Smith et al., 2014). The quantification of hydrocarbon leakage has previously been estimated from underfilled trap capacities (e.g., Donovan, 1974) or by petrophysical evaluation of paleo fluid contacts (Brincat et al., 2006; Lisk et al., 2002). Timing of leakage events has been quantified for diffusion through top seals (Krooss et al., 1992) and estimated for top seal leakage using petroleum system modelling (Ostanin et al., 2017). However, only very few studies have undertaken an explicit quantification of the volume of leaked hydrocarbons combined with an assessment of the timing of leakage (e.g., Foschi et al., 2020), and our understanding of leakage flux therefore remains very limited at present.

The primary aim of this study is to demonstrate a methodology using subsurface data to better constrain the timing and quantity of leaked hydrocarbons from a breached trap. The methodology may be adapted to apply more widely to improve assessment strategies for hydrocarbon exploration and subsurface carbon sequestration. This study is based on an integrated seismic and well data analysis of an undrilled, breached gas accumulation on the Exmouth Plateau on the North West Shelf (NWS) of Australia (Fig. 1). The NWS is a prolific hydrocarbon province with a wide range of documented leakage phenomena and subsurface fluid flow structures (Gartrell et al., 2003; O'Brien and Woods, 1995; Paganoni et al., 2019), and is this an ideal location to base such a study. The leakage phenomena in the NWS are commonly observed directly above underfilled hydrocarbon traps (Bailey et al., 2006; Foschi and Cartwright, 2020; Jablonski et al., 2013). Seismic leakage indicators are systematically described and interpreted, and placed within a structural and stratigraphic framework, to constrain the timing of leakage. Importantly, the use of amplitude mapping allows us to define present day and paleo hydrocarbon contacts, and these are used with conventional reservoir mapping to estimate the volume of leaked hydrocarbons.

2. Geological setting

2.1. Regional context

The North West Shelf (NWS) is a major hydrocarbon province offshore Australia, consisting of five basins: Bonaparte, Browse, Canning, Roebuck and Northern Carnarvon (Geoscience Australia, 2020). The Northern Carnarvon Basin can be further split into six sub-basins of which the Exmouth Plateau is one (Fig. 1). The area is characterised by a thick Mesozoic and Cenozoic sedimentary sequence (Fig. 1D) evolving from an intracratonic basin in the Palaeozoic to a rift basin in the Mesozoic and finally a passive margin (Exon et al., 1982; Exon and Buffler, 1992).

A failed rifting event linked to the early break-up of Gondwana during the Permo-Carboniferous resulted in the formation of an intracratonic sag basin across the North West Shelf (Exon et al., 1982). This

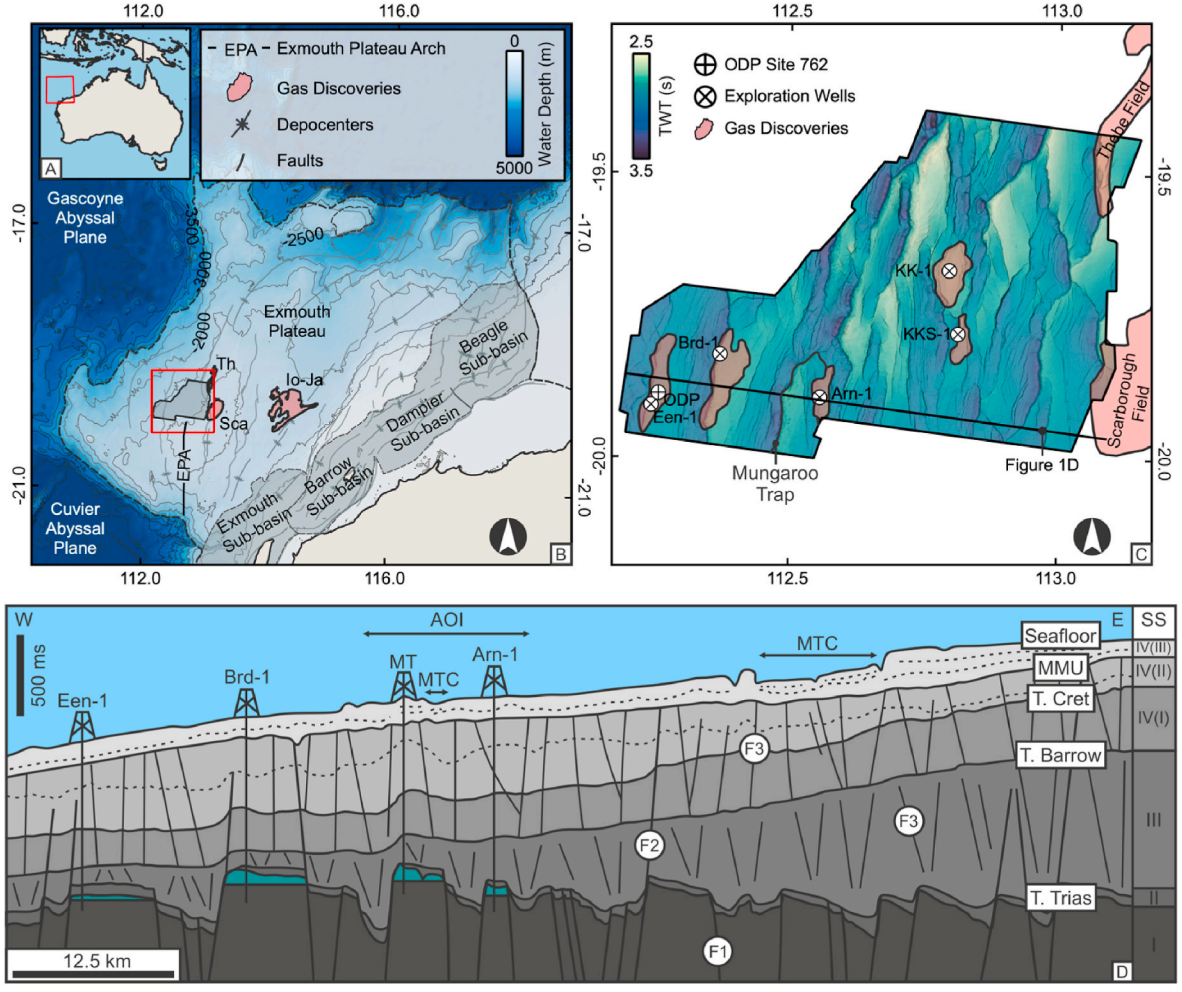

Fig. 1. (A) Map of Australia showing the location Fig. 1B (red box). (B) Bathymetry map of the Northern Carnarvon Basin. Major sub-basins, structural elements and key discoveries taken from Geoscience Australia (2020). (C) A TWT depth map of the Top Triassic. Includes the locations of ODP Site 762, and industry wells (Arnhem-1, Brederode-1, Eendract-1, Kentish Knock-1 and Kentish Knock South-1) and the Mungaroo Trap (MT). (D) Schematic cross-section across the Bonaventure 3D SS, highlighting the four megasequences (I-IV) and subunits (IV(I)-IV(III)) and three fault systems (F1-3) as well as the Mungaroo Trap (MT). (Colour, 2 column). (For interpretation of the references to colour in this figure legend, the reader is referred to the Web version of this article.)

established the basement architecture which accommodates the thick sedimentary cover. A period of tectonic stretching including two rift phases from the Late Triassic to Cretaceous. The first rift event spanned the Late and middle Jurassic from the Rhaetian to Callovian/Oxfordian, followed by a second rift phase through the Late Jurassic ending in the Tithonian. The first rift phase included uplift and normal faulting of the Triassic sediments, which were subsequently reactivated by the second rift phase (Haq et al., 1992). Extension continued into the Cretaceous with the break-up of the Argo, Gascoyne and Cuvier rifts which started in the Early Cretaceous. The North West Shelf then transitioned to a

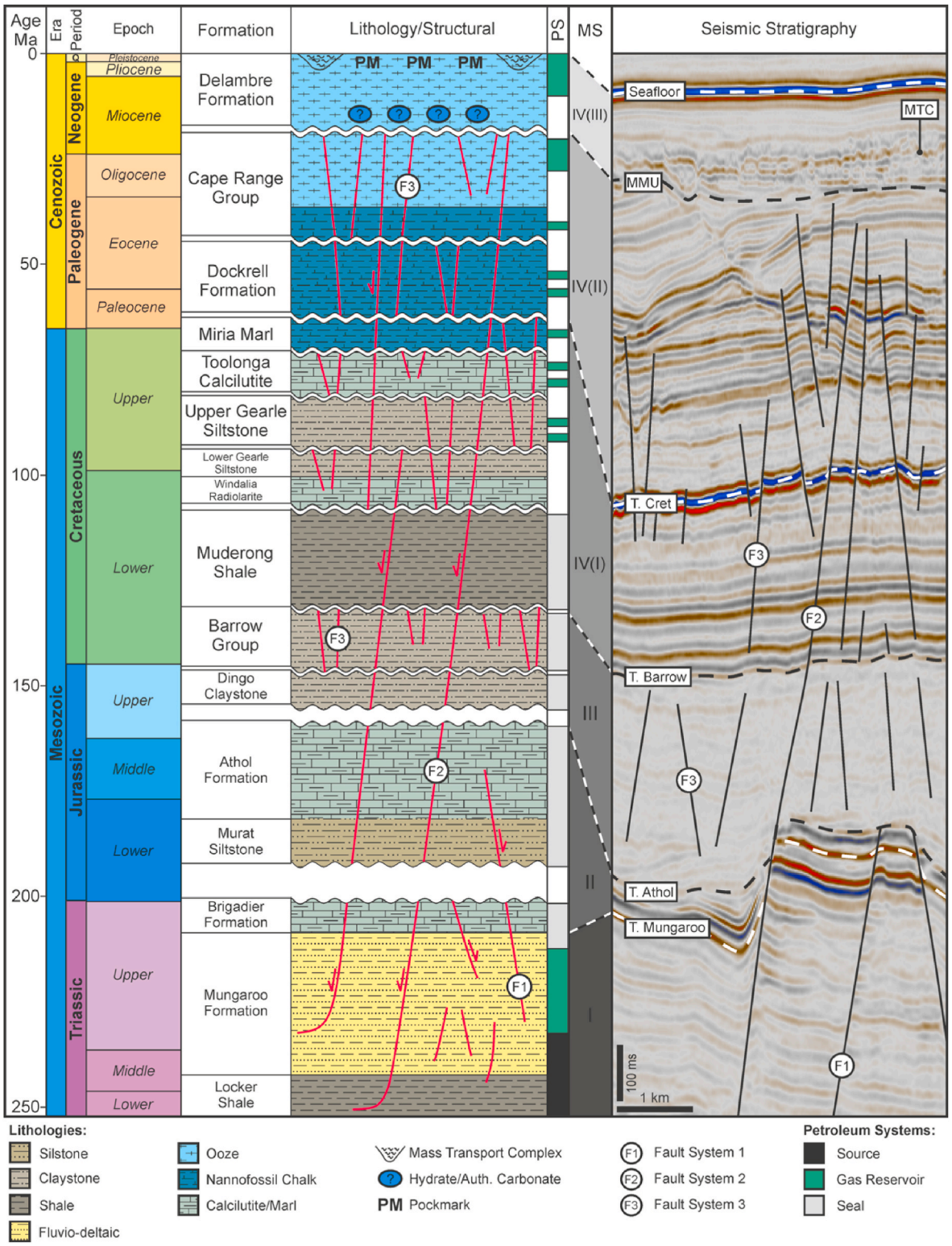

Fig. 2. A simplified tectonostratigraphic chart of the Exmouth Plateau adapted from (Bilal and McClay, 2022). Formation names and petroleum systems (PS) are based on (Paganoni et al., 2019). (Colour, 2 column). (For interpretation of the references to colour in this figure legend, the reader is referred to the Web version of this article.)

passive margin from the Late Cretaceous and throughout the Cenozoic (Exon et al., 1992). Deformation during the Neogene varies across the North West Shelf. The eastern margin was dominated by compressional tectonics whereas the Northern Carnarvon basin was characterised by a passive margin (Keep et al., 2007). However, Miocene inversion structures and folding have been observed across the NWS, including the Exmouth Plateau (Hillis et al., 2008; Müller et al., 2012). The current stress regime varies across the NWS with mean horizontal stress orientated west-northwest to east-southeast in the Northern Carnarvon Basin (Hillis et al., 2008).

The Permo-Triassic pre-rift sediments are dominated by intracratonic fluvio-deltaic, shallow marine and carbonate sedimentation (Exon and Buffler, 1992; Longley et al., 2002). These are unconformably overlain by the Early Triassic Locker Shale and Mungaroo Formations, deposited during a regional marine transgression (Fig. 2). The Mungaroo Formation is composed of fluvio-deltaic coals, claystone, siltstone and sandstones sediments. Rapid subsidence from the Late Triassic to the Early Jurassic marks the conclusion of the marine transgression with the deposition of shelfal siltstones, claystones and marls in the Brigadier Formation and Murat Siltstone (Fig. 2) (Geoscience Australia, 2020).

During the first Jurassic rift event, syn-rift sediments were deposited in low energy marine environments within fault hanging walls (Haq et al., 1992). They consist of shallow-marine clays and marls of the Athol Formation and fine grained organic rich Dingo Claystone (Fig. 2). Deposition of the Dingo Claystone continued during the second failed rifting event (Exon and Buffler, 1992). Extension and rapid subsidence in the Early Cretaceous due to seafloor spreading and the formation of the Argo Abyssal plain is marked by the Barrow Group, a thick deltaic clastic wedge corresponding to the subsequent regional marine transgression (Fig. 2) (Boyd et al., 1992). The onset of breakup along the Gascoyne and Cuvier rifts coincided with termination of clastic input and corresponds to a regional sea-level rise due to post-break up thermal subsidence. This resulted in the deposition of transgressive marine claystones, deep-water radiolarites and hemipelagic calcareous claystones (Exon et al., 1982). These correspond to the Muderong Shale, Windalia Radiolarites and the Exmouth Plateau equivalent of the Gearle Siltstone (Fig. 2).

The Late Cretaceous onset of passive margin conditions is characterised by the deposition of marly and nannofossil chalks, and other carbonate dominated sequences (Fig. 2) (Haq et al., 1990). Deposition of nannofossil and foraminifera-rich chalks and oozes are observed throughout the Cenozoic punctuated by a hiatus in the Middle Miocene, after which deposition continued to present day (Fig. 2) (Exon and Buffler, 1992).

2.2. Petroleum system

The Northern Carnarvon Basin is Australia's premier hydrocarbon province with over 672 MMbbls oil, gas and natural gas liquids produced as of May 2020 (Geoscience Australia, 2020). Over 40 gas fields have been discovered on the Exmouth Plateau the largest being the Io-Jansz and Scarborough fields (20 and 7.3 Tcf) (Fig. 1). Most wells in the nearby study area have been drilled to test Triassic tilted fault blocks within the Brigadier and Mungaroo Formations (Arnhem, Brederode and Eendracht discoveries) (Geoscience Australia, 2020) (Fig. 1).

The primary source rock within the Exmouth Plateau petroleum system is the Upper Triassic Mungaroo Formation (Fig. 2). This is a gas-prone source composed of fluvio-deltaic coals and carbonaceous claystones. A further potential secondary gas-prone source may be present in the organic-rich marine Locker Shale (Geoscience Australia, 2020). This combination has been inferred as the primary charge for the giant gas accumulations on the Exmouth Plateau (Bussell et al., 2001; Exon and Willcox, 1978).

Multiple reservoir intervals at different ages are present on the Exmouth Plateau (Fig. 2). They vary from fluvio-deltaic and shallow marine sands in the Triassic Mungaroo and Brigadier Formations to basin floor fans and turbidites in the Barrow Group (Early Cretaceous). Both Triassic and Cretaceous aged reservoirs have proved successful exploration targets across the area (Chongzhi et al., 2013; Geoscience Australia, 2020; Jablonski et al., 2013).

The Muderong Shale acts as an effective regional top seal across the Northern Carnarvon Basin (Dewhurst et al., 2002; Dewhurst and Hennig, 2003; Kovack et al., 2004). It is interpreted as a deep-water shale deposited during marine transgression that varies in thickness from 5 to >900 m (Dewhurst and Hennig, 2003; Kovack et al., 2004). Mercury Injection Capillary Pressure analysis and capillary pressure measurements show that the Muderong Shale can retain hydrocarbon column heights of 100–1000 m (Dewhurst et al., 2002; Dewhurst and Hennig, 2003; Kovack et al., 2004). Intra-formational shales form local seals and stacked reservoir formations in the deeper Barrow Group, Dingo Claystone, Brigadier Formation and Mungaroo Formation (Bussell et al., 2001; Dewhurst et al., 2002).

On the Exmouth Plateau, hydrocarbon generation from the source rocks of the Mungaroo Formation is predicted to have begun in the Late Triassic to Early Jurassic and continued throughout the Cenozoic (Cook et al., 1985). At the present-day, peak gas expulsion is modelled at depths of 5000 m below the seafloor (Barber, 1982; Bussell et al., 2001). The Northern Carnarvon Basin is characterised by good access to charge. Hydrocarbon column heights of over 100–200 m are commonly observed, rising to above 500 m at Dixon-1 and North Rankin-1 (Jablonski et al., 2013).

Leakage phenomena and underfilled traps have been well documented on the North West Shelf (Bailey et al., 2006; Jablonski et al., 2013; O'Brien et al., 2005). Phenomena identified have included pockmark craters, hydrocarbon-related diagenetic zones (HRDZs), shallow gas amplitude anomalies and seafloor mounds (Cowley and O'Brien, 2000; O'Brien and Woods, 1995; Rollet et al., 2006). The phenomena have clustered and linear spatial distributions and have been linked to fluid migration in response to tectonic and polygonal faulting, sediment remobilization, gas chimneys, pipes and hydrate dissociation (Gartrell et al., 2004; Imbert and Ho, 2012; Magee et al., 2016; Seebeck et al., 2015). Within the Exmouth Plateau, both present-day seafloor pockmarks and paleo-pockmarks affecting Jurassic and Triassic datums have been observed (Cowley and O'Brien, 2000; Riera et al., 2022; Velayatham et al., 2018) along with fluid flow indicators including seismic chimneys, pipes, sediment remobilization structures and fault related migration (Dirnstein et al., 2013; Mercado Ruge et al., 2020; Paganoni et al., 2019).

3. Data and methods

The study area is located on the Exmouth Plateau in 900–1580 m water depths (Fig. 1). The database used combines a three-dimensional (3D) post-stack, time migrated seismic volume with borehole calibration from the Ocean Drilling Program (ODP Site 762) and five petroleum exploration wells (Arnhem-1, Brederode-1, Eendract-1, Kentish Knock-1, Kentish Knock South-1) (Fig. 1).

3.1. Seismic data

The 'Bonaventure 3D MSS' seismic cube is a full-stack volume acquired by WesternGeco in 2006 with an aerial extent of ~4300 km^2. The volume was acquired with an inline and crossline spacing of 18.5 m and 12.5 m, respectively and processed to 0° phase (North American polarity) with a sample interval of 4 ms. Within the shallow subsurface the dominant frequency is 45–55 Hz. Using interval velocities of 1700 and 2500 m s^{-1}, and a dominant frequency of 50 Hz, the vertical resolution (quarter of the dominant wavelength) is ~8 m and ~11 m (Widess, 1973).

3.2. Well data

Borehole data from the five petroleum exportation wells were used to constrain the regional distribution of reservoir properties (Table 3) and provide calibration for the mapping of regional two-way-time (TWT) surfaces, interpreted by Paganoni et al. (2019). Further calibration and dating of the shallow Cenozoic stratigraphy was provided by ODP Site 762 (Leg 122) (Haq et al., 1990).

The offset Arnhem-1 well was used to provide localized constraints closer to the study area. This included the velocity model used for the depth converting surfaces interpreted in this study, seal properties and fluid properties. Arnhem-1 was selected due to its proximity to the Mungaroo Trap, ~3.5 km to the east in an adjacent tilted fault block (Fig. 1). To test the validity of Arnhem-1 as a control well, a well-to-seismic calibration was used (Fig. 4). A pseudo-well seismic trace was generated at the crestal position of the breached trap and compared with the seismic and synthetic traces at Arnhem-1 (Fig. 4). A strong correlation between the top seal and upper reservoir units was observed (Fig. 4).

A layer cake velocity model (Brown, 2011) using the regional TWT surfaces interpreted by Paganoni et al. (2019) and velocity data from Arnhem-1 was used for depth conversion. The regional surface included: Seafloor, Mid-Miocene Unconformity (MMU), Top Cretaceous, Top Barrow Group, Top Athol and Top Mungaroo (Fig. 2).

Seal capacity properties were obtained from fracture gradients measured using leak-off tests (LOTs) within the Barrow Group and the drilling mud weight at Arnhem-1 (Allen et al., 2013) (Fig. 3). The fracture pressure at the top seal interval within the study area was predicted by linearly extrapolating the fracture gradients from Arnhem-1 to the depth of the top reservoir in the study area (Fig. 10).

3.3. Seismic interpretation of fluid flow

Seismic interpretation was carried out using acoustic amplitude, as well as RMS Amplitude (route mean square) and coherency attribute volumes. In this study, an increase of acoustic impedance with depth is interpreted as a hard reflection and is characterized by a positive excursion of the central loop of the seismic wavelet. Conversely, a decrease of acoustic impedance with depth is interpreted as a soft reflection and is characterized by a negative amplitude.

AAs were interpreted from an increase in amplitude of the background reflectivity profile indicating a change in acoustic impedance (Brown, 2011; Cox et al., 2020; Sheriff, 1975). In this study, Hard AAs are interpreted as positive amplitude increases that denote an increase in acoustic impedance. A Soft AA is interpreted as a negative increase in amplitude denoting a decrease in acoustic impedance.

The focused fluid flow structures in this study were interpreted using criteria set out by Andresen (2012); Hustoft et al. (2007); Ligtenberg (2005) and Løseth et al. (2009). Pockmarks are defined as crater-like erosive features indicating removal of sediment at the present/paleo-seafloor (Gay et al., 2006; Hovland and Judd, 1988). Vertical fluid flow structures, including fluid escape pipes and gas chimneys, are characterized as zones of decreased coherency and reduced amplitude (Gay et al., 2012; Heggland, 1997; Hustoft et al., 2007; Løseth et al., 2011). Stacked soft amplitude anomalies were interpreted as due to free gas accumulating within the pore space (Bünz and Mienert, 2004; Heggland, 1997).

3.4. Reservoir volumetric calculations

Standard deterministic volumetric calculations (Jahn et al., 2008) using the position of the fluid contacts were used to calculate the volume of methane within the leaking trap. To account for lateral facies variations between Arnhem-1 and the study area we compiled reservoir properties from all five exploration wells within the Bonaventure 3D seismic survey area (Table 3). A truncated normal distribution for

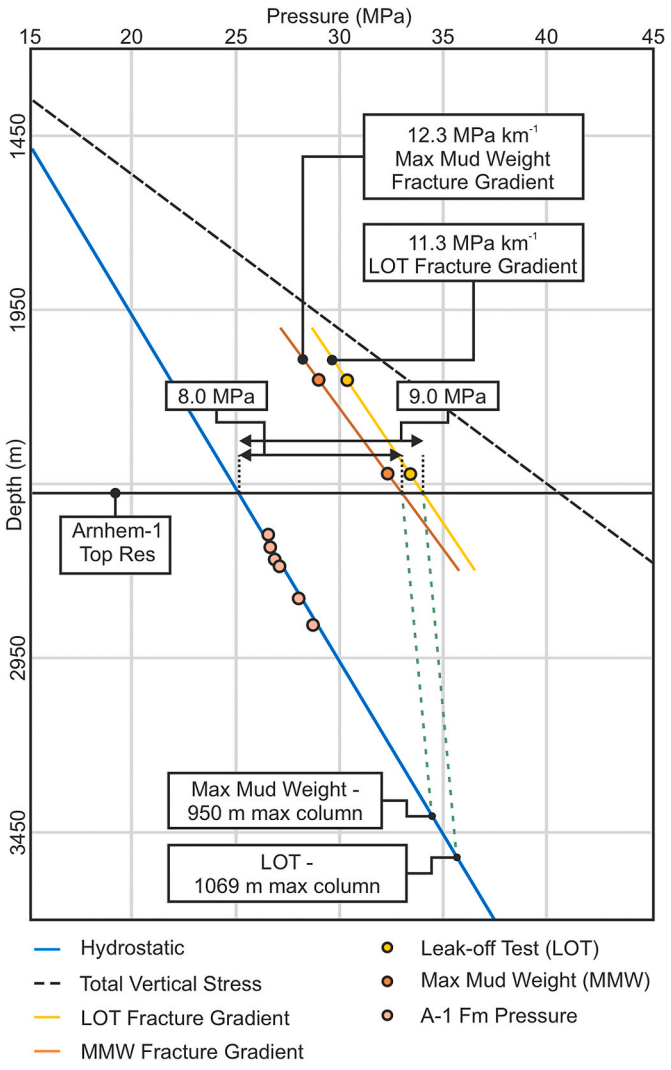

Fig. 3. Pressure depth plot showing the subsurface pressure measurements (Allen et al., 2013), fracture gradients and inferred seal capacities at Arnhem-1. Extrapolating the Max Mud Weight (MMW) and Leak-off Test (LOT) fracture gradients to the depth of the Arnhem-1 Top Reservoir shows that 8.0 MPa (MMW) and 9.0 MPa (LOT) of overpressure is required to induce hydraulic fracturing of the top seal. From these overpressures the seal capacity at Arnhem-1 can be inferred as 950 m (MMW) and 1069 m (LOT). (Colour, 1 column). (For interpretation of the references to colour in this figure legend, the reader is referred to the Web version of this article.)

reservoir net-to-gross and porosity values centred on the mean value from the industry well measurements (Fig. 9) and a linear distribution of water saturations measured from the industry wells was used as input for a Monte Carlo simulation of the reservoir volume (Fig. 9).

4. Results

4.1. Structural and seismic stratigraphic framework

The stratigraphic and structural framework of the Exmouth Plateau has been comprehensively described by Bilal and McClay (2022). In this study we follow both their megasequence subdivision and their classification of three main fault systems. Consequently, the stratigraphy of the study area has been subdivided into four megasequences: I – pre-rift; II –syn-rift; III - post-rift; and IV - present-day passive margin strata.

The three major fault systems classified by (Bilal and McClay, 2022) were mapped across the study area. Fault System 1 formed through

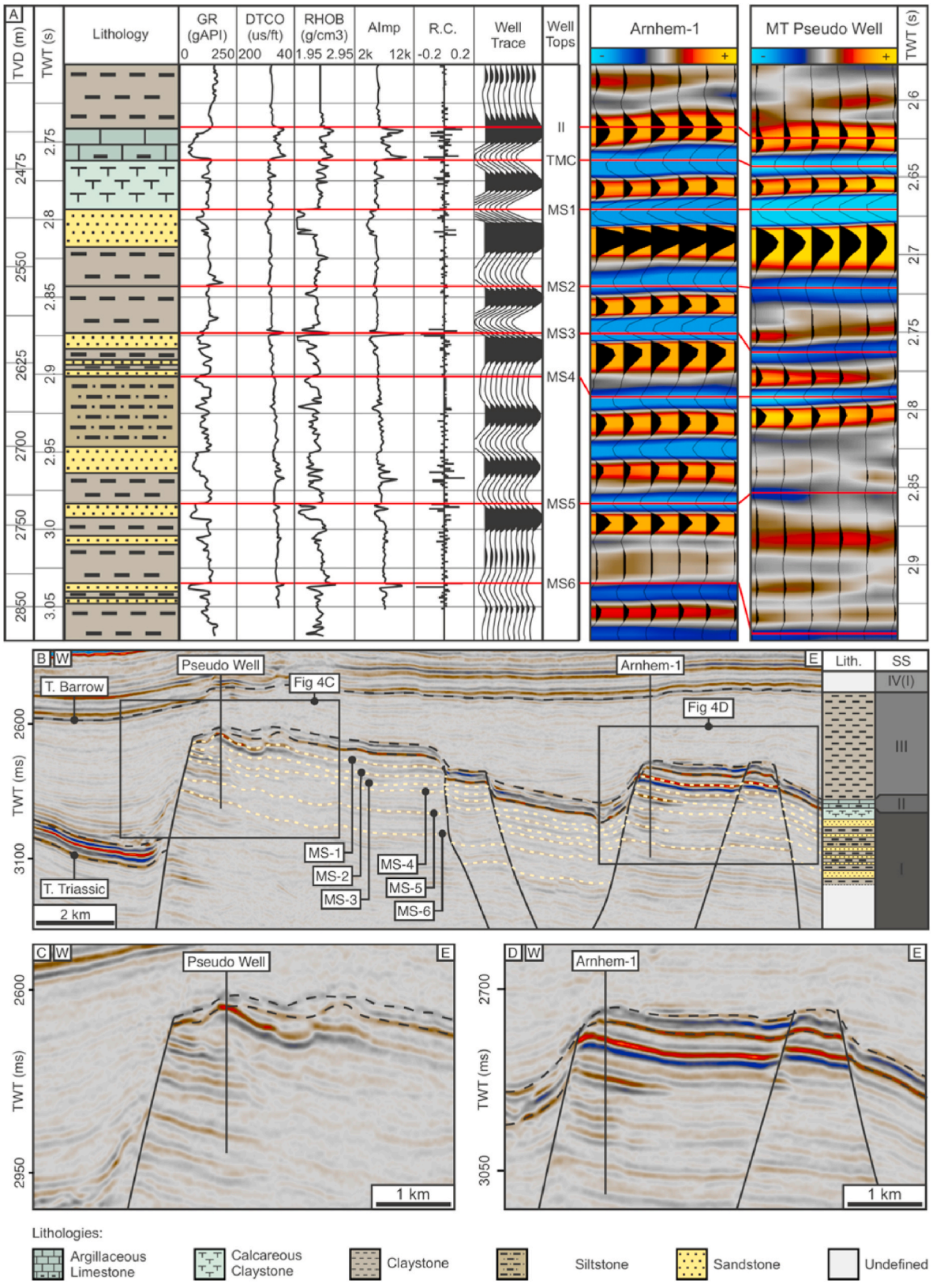

Fig. 4. (A) Seismic well tie comparing Arnhem-1 to the Pseudo Well at the crestal point within the Study Area. Well logs are taken from the Arnhem-1 seismic tie (Allen et al., 2013) and compared to the seismic extracted at Arnhem-1 and a pseudo well at the crest of the Mungaroo Trap. The results are flattened on the Top Mungaroo Claystone (TMC) to minimise the effects of lateral thickness variations in the shallower overburden. (B) A seismic section showing the correlation of the seal and reservoir horizons from Arnhem-1 to the study area. Magnification of the uninterpreted seismic (B) highlighting the reservoir units and DHIs at (C) the Pseudo Well and (D) Arnhem-1. (Colour, 2 column). (For interpretation of the references to colour in this figure legend, the reader is referred to the Web version of this article.)

Mesozoic extension forming large N–S to NNE-SSW trending extensional faults that form rotated fault block structures (F1 – Figs. 1D and 2). The faults are predominantly west-dipping faults with smaller antithetic faults that dip to the east. Fault System 2 formed through reactivation of the deeper Fault System 1 during the Early Cretaceous to Neogene and consists of NNE-SSW trending segmented normal faults within the Cenozoic interval (Bilal and McClay, 2022) (F2 – Figs. 1D and 2). Fault System 3 consists of two stacked tiers of non-tectonic polygonal faults within Megasequences III & IV (F3 – Figs. 1D and 2).

Megasequence I consists of the Locker Shale and Mungaroo Formation (Fig. 2). The sequence is characterised by parallel seismic reflections dipping to the SE ~1.5° within the tilted fault blocks (Fig. 2).

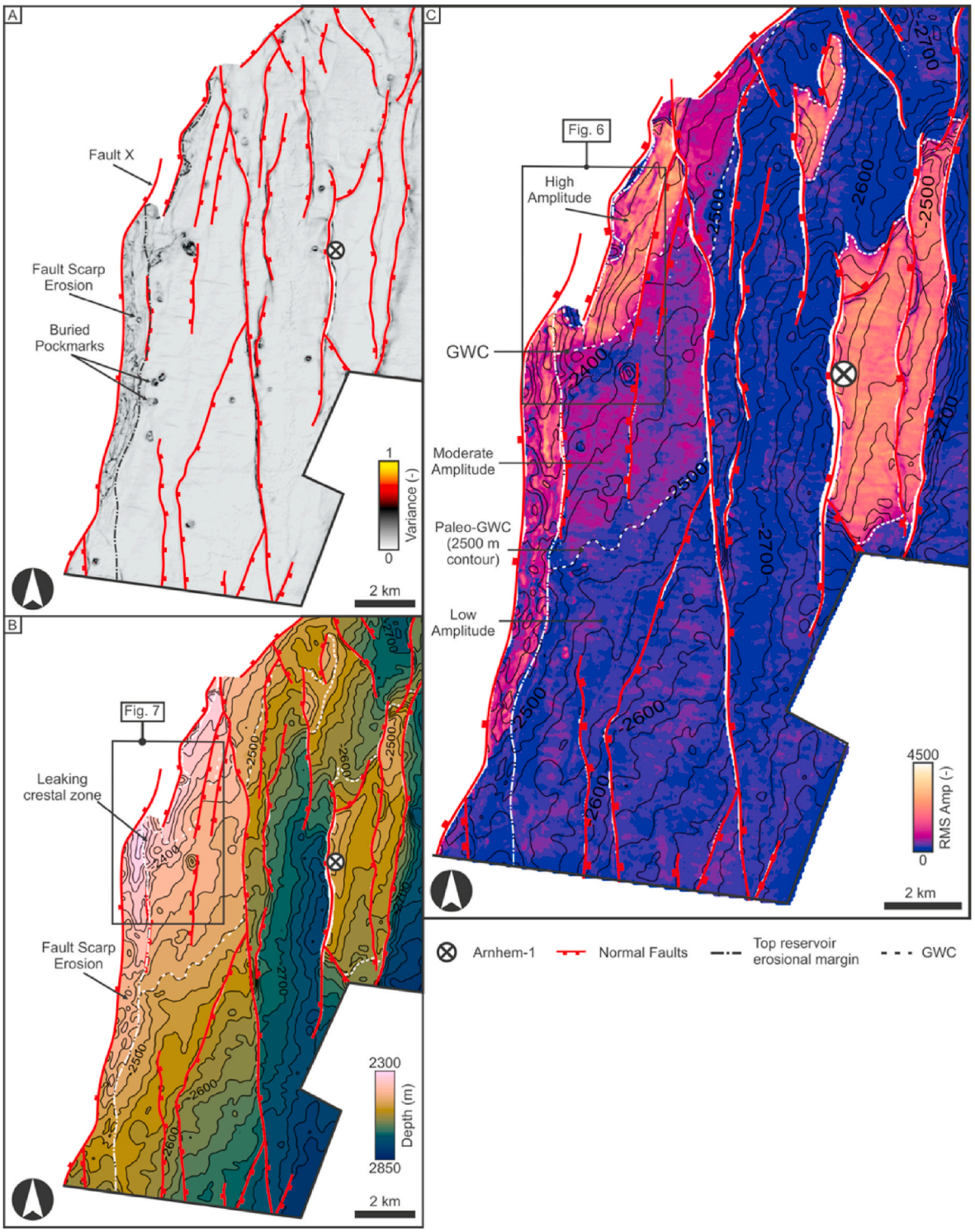

Fig. 5. (A) A seismic coherency map extracted along the Top Triassic surface across the Mungaroo Trap and Arnhem discovery. The attribute highlights the position of the normal faults, buried pockmarks and fault scrap erosion. (B) Depth structure map of the Top MS1 Reservoir, showing the position of the inferred gas-water contacts (GWCs). (C) A seismic amplitude extraction along the Top MS1 Reservoir Horizon showing the position of the three amplitude domains (high, moderate and low) and the inferred GWCs. (Colour, 2 column). (For interpretation of the references to colour in this figure legend, the reader is referred to the Web version of this article.)

Areas of increased amplitude are distributed throughout the tilted fault blocks highlighting potential direct hydrocarbon indicators (DHIs) (Figs. 2 and 4). The top of this megasequence displays multiple craters within the top of the Mungaroo Formation (Fig. 5A). These have been described as fluid escape pockmark craters or pit chain craters related to igneous dyke emplacement (Dirnstein et al., 2013; Magee and Jackson, 2020; Velayatham et al., 2019).

The syn-extension Megasequence II contains the Brigadier and Athol Formations. The sequence is a laterally continuous drape over the underlying Mungaroo Formation (Figs. 1 and 2). The sequence varies in thickness across the dataset from ~50 m on fault block highs to 200 m within the fault hanging walls, where the deposits form in wedge shaped packages (Fig. 2). Significant fault scarp degradation can be observed, incising through the Brigadier Formation into the Mungaroo Formation below (Bilal et al., 2020; Bilal and McClay, 2022) (Fig. 5A).

Megasequence III is characterised by a seismically transparent wedge with little internal reflectivity (Fig. 2). The sequence geometry dips westwards but drapes the underlying Triassic fault block structure, growing thicker in the hanging walls and thinning over the fault block highs (Paganoni et al., 2019) (Fig. 2). This corresponds to the Barrow Group claystones (Allen et al., 2013) (Fig. 2).

Megasequence IV is dominated by the passive margin sedimentary fill. This is comprised of the Muderong Shale, Windalia Radiolarite, Cretaceous nannofossil chalks and Cenozoic oozes (Fig. 2). The thickness of the sequence varies between 700 and 1000 m controlled by the underlying rotated fault blocks (Fig. 2). This megasequence is divided into three subunits for this case study (Fig. 2):

Unit I manifests as a laterally continuous reflections draping Meagsequence III (Fig. 2) and comprises the Muderong Shale, Windalia Radiolarite and Gearle Siltstone. The seismic amplitude response varies from moderate within the Muderong Shale at the base to low amplitude within the Windalia Radiolarite and Gearle Siltstone above. The top of the Unit 1 is represented by a high amplitude, hard reflection that is laterally continuous across the dataset (Fig. 2) which is dated as the Cretaceous-Cenozoic boundary (Haq et al., 1990).

The base of Unit II is characterised as a package of low amplitude laterally continuous reflections (Fig. 2). These correspond to Paleocene nannofossil chalks (Haq et al., 1990). Above these is a package of contourite deposits with mounded geometries (Nugraha et al., 2019; Paganoni et al., 2019) (Fig. 2). The top of the contourite package is separated from Unit III by the Mid-Miocene Unconformity (Haq et al., 1990; Paganoni et al., 2019) (Fig. 2).

Unit III is characterised by a package of low amplitude, laterally continuous sub-parallel reflections (Fig. 2). These dip shallowly to the NW and are generally concordant with the present-day seafloor. This package is interpreted as consisting of Pliocene to Quaternary nannofossil oozes (Haq et al., 1990), and has a predominantly low amplitude response. The seafloor itself is an unconformity surface with Late Pleistocene sediments occurring just below the surface as calibrated by ODP 762 with a probable age of 290 Ka (Haq et al., 1990; Young, 1998).

The present-day seafloor and shallow subsurface are disrupted by mass transport complexes (MTCs) displayed as discontinuous and chaotic reflections with increased amplitude (Scarselli and Elders, 2013) (Fig. 2). The MTCs align in southeast-northwest trending flow corridors that remain active at the present day forming steep arcuate headscarps and erosional remnant highs on the seafloor (Scarselli and Elders, 2013). The present-day seafloor also shows signs of small crater shaped depressions that cluster together on the erosional remnant highs and at the margins of the MTCs (Paganoni et al., 2019; Scarselli and Elders, 2013).

4.2. Trap, seal and reservoir characteristics

The hydrocarbon accumulation that is the primary focus for this study is a combination structural -stratigraphic trap. This consists of stacked reservoir units within a tilted fault block formed by Fault Systems 1 and 2 (Fig. 1) and where there is a component of stratigraphic trapping (lateral truncation) provided by scarp degradation of the major fault bounding the tilted fault block. For ease of description, it is referred to here as the 'Mungaroo Trap'.

4.2.1. Trap

The Mungaroo Trap consists of interbedded stacked reservoir units of the Mungaroo Formation (Fig. 4). The focus of this study is the uppermost reservoir unit (MS1 – Fig. 4), which is stratigraphically trapped along most of its up dip lateral margins and sealed laterally and vertically by claystones of the Mungaroo and Barrow Groups (Fig. 4). These provide an onlap juxtaposition with MS1 against the highly eroded fault scarp of the NNE trending, block-bounding fault (Figs. 2 and 4). The northern limit of the trap is a fault juxtaposition lateral seal against the Mungaroo and Barrow Group claystones (Fig. 5).

The full extent of the structural closure of the Mungaroo Trap is not known because it extends to the south of the Bonaventure 3D survey coverage (Fig. 1). A minimum areal extent of c. 100 km^2 can be mapped to a down flank limit at ~2800 m (Fig. 5). The crest of the Mungaroo Trap at MS1 is 2360 m (Fig. 5), giving a minimum trap capacity at this uppermost reservoir of 440 m.

4.2.2. Seal characteristics

The immediate top seal for MS1 is the Top Mungaroo Claystone (TMC) (Allen et al., 2013). Cuttings descriptions and well data from Arnhem-1 show the TMC to be ~40 m thick, comprising claystones with thin silty claystone interbeds (Allen et al., 2013). The TMC is overlain by the Brigadier and Athol Formations in Megasequence II acting as additional seals (Allen et al., 2013). The lateral seal is a combination of onlap or fault juxtaposition with the claystones of the Barrow Group (Fig. 4).

Hydraulic seal capacity can be used to describe the maximum column height a seal can support before failure through hydrofracturing (Watts, 1987). This can be used to calculate the maximum hydrocarbon column height. At Arnhem-1 Leak-off tests (LOT) and maximum mud weight (MMW) data measured within the Barrow Group yielded estimated fracture gradients of 11.3 MPa km^{-1} and 12.3 MPa km^{-1} for the overburden and sealing units (Fig. 3) (Allen et al., 2013). Given these fracture gradients, the overpressure required to hydraulically fracture the top seal at Arnhem-1 is 9.0 MPa (based on LOT) and 8.0 MPa (based on MMW) (Fig. 3). The hydraulic seal capacity of the top seal at Arnhem-1 is therefore 1069 m (based on LOT) and 950 m (based on MMW) (Fig. 3).

4.2.3. Reservoir characteristics

The Triassic reservoirs proven in the Arnhem-1 well comprise a total of six shallow marine-deltaic sands interbedded with marine shales (Allen et al., 2013) (MS1-6, Fig. 4), of which the uppermost five were gas bearing (Allen et al., 2013). The net pay of these five gas sands is ~50 m over a ~350 m thick interval (Allen et al., 2013).

Core and petrophysical analysis at Arnhem-1 shows the total porosity across the reservoir horizons varies between 0.27 and 0.32 v/v and water saturation between 0.24 and 0.47 v/v (Table 1) (Allen et al., 2013). Permeability varies depending on the depositional facies from 800 to 5900 mD (Table 1) (Allen et al., 2013). Six unique gas gradients were identified in the Mungaroo reservoirs implying that these six

Table 1
Summary of the reservoir properties from the gas bearing Mungaroo reservoir horizons taken from Arnhem-1 (Allen et al., 2013).

Unit	Res. Thickness (m)	Net:Gross (v/v)	Porosity (v/v)	Permeability (mD)	Water Saturation (v/v)
MS1	19.7	0.85	0.32	801	0.24
MS2	2.7	0.62	0.28	821	0.34
MS3	25.6	0.5	0.29	920	0.47
MS4	11	0.51	0.29	1850	0.43
MS5	10.2	0.92	0.3	5972	0.28

stacked reservoir units are not in vertical pressure communication (Allen et al., 2013). Each reservoir is normally pressured with a gas density of 170 kg m^{-3} (Allen et al., 2013).

4.3. Reservoir amplitude characteristics

The five gas bearing reservoir units proven in Arnhem-1 (Allen et al., 2013) each correspond to individual stratal reflections within the seismic data (Allen et al., 2013) (Fig. 4). All five reflections are associated with high amplitude soft anomalies where there is a significant amplification of the background (down flank) amplitude values (Fig. 4). The most prominent anomaly is associated with the shallowest reservoir unit, MS1 (Figs. 4 and 5C).

A detailed study of the amplitude response of the shallowest reservoir unit (MS1) was conducted in the area encompassing the Mungaroo Trap and the Arnhem gas discovery (Fig. 5C). The MS1 horizon displays unambiguous evidence of a soft amplitude anomaly within the crestal zone of the Arnhem discovery (Fig. 5). The high amplitude soft anomaly observed at Arnhem-1 is calibrated by logs and by fluid analysis to be gas bearing with a 76% gas saturation (Allen et al., 2013).

Similar soft amplitude anomalies are mapped over the most up dip portion of the closed area of the Mungaroo Trap as seen in profile (Fig. 4B and C) and on the amplitude map of the MS1 horizon (Fig. 5C). The RMS amplitude extraction along the MS1 horizon shows three distinct amplitude regions (low, moderate, and high) distributed across the study area (Fig. 5C). The high amplitude regions coincide with the structurally highest regions of the faulted MS1 horizon at the Mungaroo Trap and the Arnhem discovery. The high amplitude regions have sharp well-defined margins between the anomalies and the almost uniform background low amplitude regions (Fig. 5C). The up-dip margins of both traps conform to the juxtaposition with reservoir bounding faults (Fig. 5C). At the Arnhem discovery, the down-dip margins of the high amplitude regions conform to the 2600 m depth structure contour (Fig. 5C). In contrast, along the southern and southeastern margin of the Mungaroo Trap, the high amplitude region has a boundary with a patchy, moderate amplitude region (Fig. 5C). The margin between these two areas of contrasting amplitude response does not conform to structure, and instead crosses between the 2380–2440 m structural contours over 1.6 km (Fig. 6). The moderate amplitude region is only observed within the Mungaroo Trap (Fig. 5C). The boundary between the moderate amplitude and low amplitude regions conforms closely to the 2500 m structural depth contour (Fig. 5C).

4.3.1. Interpretation of the MS1 reservoir amplitude characteristics

The pseudo well at the crest of the Mungaroo Trap and Arnhem-1 display a strong correlation in the critical interval between the TMC and the uppermost Mungaroo Reservoir (MS1) (Fig. 4). Due to the close correlation of amplitude and frequency response (Fig. 4), the high amplitude region of the MS1 amplitude map in the Mungaroo Trap is also interpreted to be gas bearing with a similar saturation to that calibrated at Arnhem-1. The sharp amplitude contact between high and low amplitude regions at Arnhem-1 is interpreted as a present-day gas-water contact (GWC) (Fig. 5C). This represents the boundary between high gas saturation reservoir and water bearing reservoir, with a concomitant return from elevated soft amplitudes to the background values.

The moderate amplitude region seen down flank from the high amplitude crestal region of the Mungaroo Trap is more ambiguous. The conformance to structure of the boundary between the moderate and background low amplitude regions (Fig. 5C) suggests that the moderate amplitudes are a fluid substitution response rather than a sedimentary facies change. A similar acoustic response on amplitude maps has been identified elsewhere with the addition of calibration with well data and seismic modelling, and has been interpreted as residual gas trapped above a paleo-gas-water contact (paleo-GWC) (Gutierrez, 2022; Medouri et al., 2015). By analogy with these studies, we interpret this patchy, moderate amplitude region to represent residual gas and hence the boundary with the low amplitude region as a paleo-GWC.

4.4. Evidence of leakage phenomena

A suite of seismic leakage indicators has been observed within the study area, exclusively clustered directly above the crestal region of the Mungaroo Trap (Fig. 7A). These leakage indicators are collectively grouped together to form a distinctive leakage zone that is distributed within the overburden from the MS1 reservoir unit up to and including present-day sea floor. The main types of leakage indicator are briefly described below, and their dimensions and diagnostic characteristics are summarised in Table 2.

The leakage zone above the Mungaroo Trap coincides with a headscarp at the modern sea floor that was formed by the development of a large mass transport complex (Bonaventure Complex II, Scarselli and Elders (2013)). A prominent cluster of 23 crater shaped depressions with crudely circular planforms is also mapped at the modern seafloor (Fig. 7D), whose dimensions are summarised in Table 2.

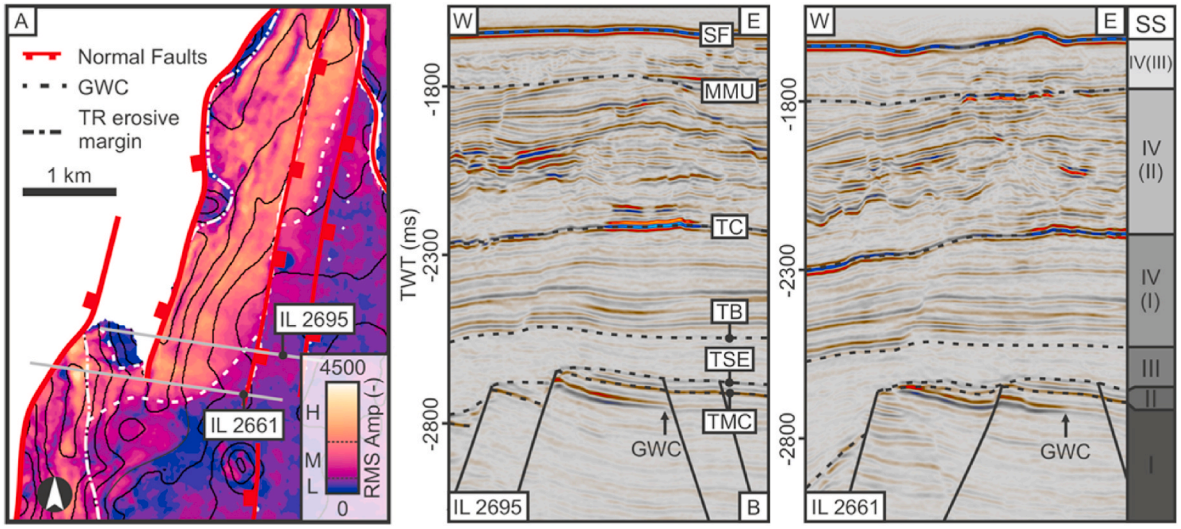

Fig. 6. (A) Zoom of the amplitude extraction of the Top Reservoir at the Mungaroo Trap showing the GWC cross-cutting multiple structural contours. (B) Seismic cross-sections from IL 2695 and 2661 demonstrating good quality data with no seismic artefacts affecting the imaging of the GWC. (Colour, 1.5 column). (For interpretation of the references to colour in this figure legend, the reader is referred to the Web version of this article.)

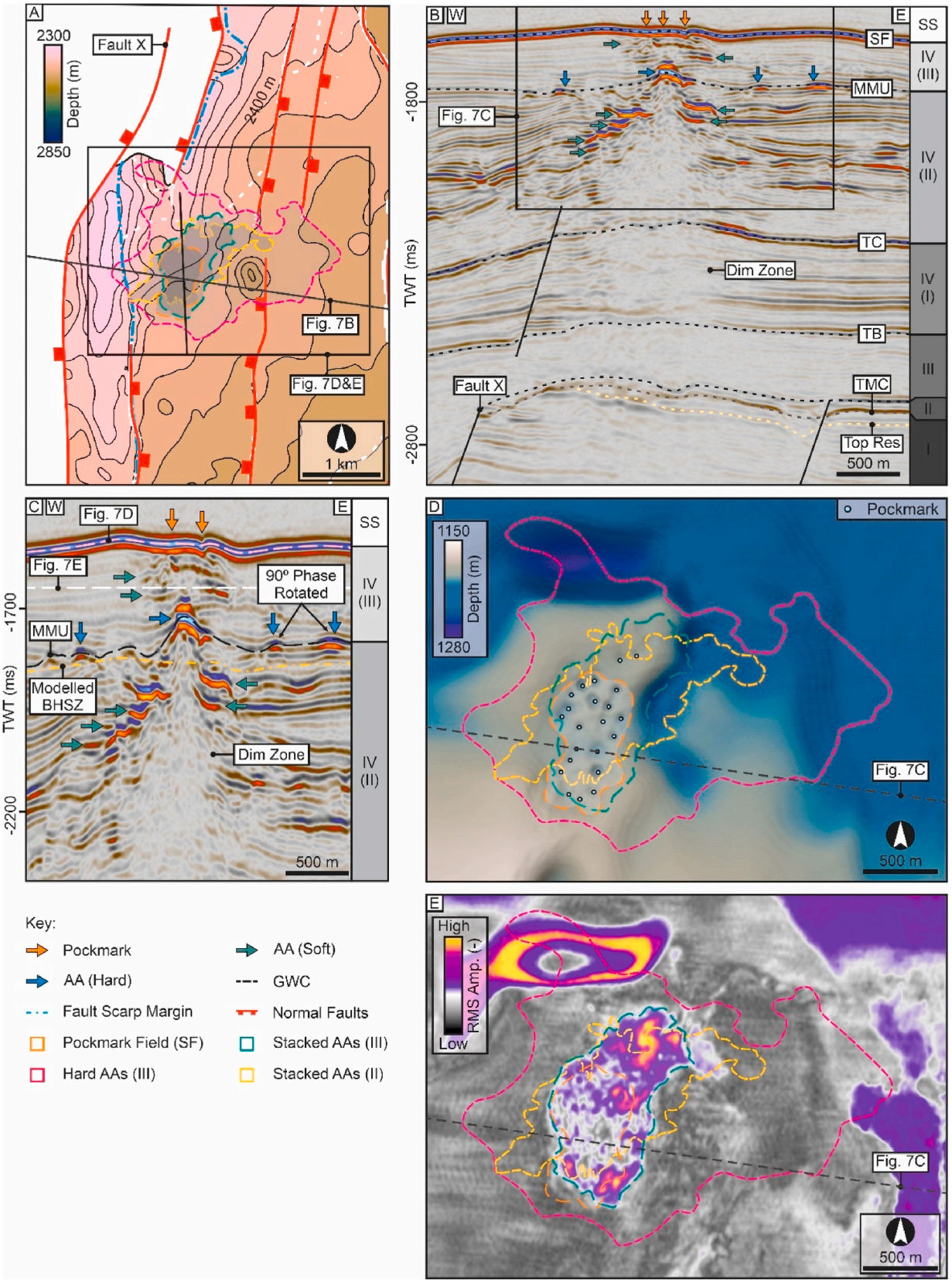

Fig. 7. (A) Zoom of the depth structure map of the Top Reservoir. Shows the positions of the leakage phenomena stacking vertically above the leaking crestal zone. (B) Seismic section from showing the distribution of leakage phenomena above the Mungaroo Trap relative to Fault X and Dim Zone. (C) Magnified seismic cross-section from (B) Highlighting the pockmark craters, amplitude anomalies and dim zone and showing the position of the base hydrate stability zone (60 °C km-1 geothermal gradient) modelled by Paganoni et al. (2019). (D) A seafloor depth map showing the position (E) An RMS amplitude extraction showing the margin of the stacked soft AAs in Unit IV(III) relative to the margins of the other leakage phenomena.

Table 2
Summary of leakage phenomena in the overburden above the Mungaroo Trap.

Unit	Leakage Indicators	Seismic Characteristics	Dimensions	Additional Information	Interpretation
Seafloor	Pockmark	23 crater shaped depressions	20–100 m in length 1–6 m erosional relief	Circular/subcircular planform geometries No clear alignment Cover an elliptical area 0.6 km^2	Seafloor pockmarks (Judd and Hovland, 2007; O'Brien et al., 2003)
IV(III)	Soft AA	Negative amplification of background reflectivity	~100 m length (individual) ~1.2 km length (coalesced)	Coalesce to form elliptical geometry with irregular crenulated margin	Free gas accumulations Bünz and Mienert (2004)
	Hard AA	Positive amplification of background reflectivity Evidence of 90° phase rotation	~80–500 m (individual) 10 km length (coalesced)	Coalesce to form patchy anomaly with irregular crenulated margin Isolated AAs distributed to west of coalesced anomaly Covers 3.2 km^2 area	Hydrate related AAs (Massive hydrate or authigenic carbonate) (Paganoni et al., 2019; Sassen et al., 2001)
IV(II)	Soft AA (Stacked)	Negative amplification of background reflectivity	~100–300 m (individual) ~6 km length (coalesced)	Vertically Stacked Coalesce to form irregular planform geometry Cover 1.0 km^2 area	Free gas accumulations (Foschi et al., 2014; Traynor and Sladen, 1997)
II to IV (II)	Dim Zone	Reduced seismic amplitude Reduced reflection coherency Convex upwards reflections	Conical shape 50 m–1000 m Convex reflections max ~40 m relief	Forms in a conical region emanating down from Hard AAs Unit IV(III) Top of dim zone has an irregular topography Top of dim zone delineates the margin between the hard AAs above and soft AAs below	Zone of vertical fluid migration (Seismic chimney, pipes, or exploitation of fracture network) (Gay et al., 2012; Heggland, 1997; Hovland and Judd, 1988)

Table 3
Summary of MS1 horizon reservoir properties measured from the petroleum industry wells covered by the Bonaventure 3D Seismic Survey.

Well	Net Reservoir (m)	Net:Gross (v/v)	Porosity (v/v)	Water Saturation (v/v)
Arnhem-1	19.7	0.85	0.32	0.24
Brederode-1	10.3	0.61	0.35	0.42
Eendract-1	17.5	0.77	0.35	0.1
Guardian-1 (Kentish Knock-1)	28.0	0.39	0.38	0.35
Kentish Knock South-1	44.7	0.93	0.34	0.22
Mean	24.0	0.71	0.33	0.27
Standard Deviation	13.1	0.21	0.05	0.12

Several soft AAs are mapped vertically below the seafloor pockmark field at the top of Unit III (Fig. 7C), and manifest as a simple amplification of the background reflectivity within Unit III (Fig. 7C). The AAs coalesce together forming a larger, elliptical amplified zone (Fig. 7E).

Several hard AAs are mapped at the base of Unit III, including a prominent set that are positioned vertically below the soft AAs and seafloor craters (Fig. 7C). The hard AAs manifest as positive amplification of the background reflectivity although some phase rotated from 0 to 90° is evident (Fig. 7C). Individual anomalies sometimes coalesce to form larger amplified region with a patchy distribution (Table 2).

Multiple soft AAs are mapped in Unit II with the same acoustic characteristics as those at the top of Unit III (Fig. 6C). The anomalies coalesce to form an amplified zone with an irregular planform geometry and irregular crenulated margin (Table 2). The soft AAs are vertically stacked below the hard AAs in the unit above (Fig. 7).

The stacked soft amplitude anomalies in Unit II are distorted by a dim zone of attenuation and amplitude blanking emanating downwards from the base of Unit III to the Mungaroo Trap (Fig. 7B). The dim zone is defined by a conical region that widens downwards towards the Top Barrow Group horizon (TB on Fig. 7B). Seismic frequency and coherency are reduced within the dim zone with seismic reflectors exhibit a convex upwards geometry (Fig. 7C). The top of the dim zone has an irregular topography and delineates the transition from hard amplitude anomalies within Unit III to soft amplitude anomalies within Unit II (Fig. 7C).

4.4.1. Interpretation of the leakage zone

The geometry and seismic expression of the craters at the present-day seafloor are consistent with that of small to medium sized pockmarks (Judd and Hovland, 2007). They are similar to previously described small pockmark fields on the Exmouth Plateau by O'Brien et al. (2003).

The vertically stacked soft AAs within Units II and III are similar to those interpreted as being related to free gas accumulations by Bünz and Mienert (2004) and Traynor and Sladen (1997), and we follow this interpretation here. Vertically stacked soft AAs developed in deep marine sediments have been attributed to multi-storey gas migration driven by capillary invasion within a strongly heterogeneous layered stratigraphy where there is a large contrast in vertical and horizontal permeability (Foschi et al., 2014).

Previous explanations for the development of hard AAs above vertical hydrocarbon leakage zones have included hydrocarbon related diagenetic zones (HRDZs) consisting of authigenic carbonates derived from methane (Cowley and O'Brien, 2000; O'Brien and Woods, 1995), or the development of high saturation gas hydrate or authigenic carbonate cements linked to natural gas hydrate systems (Petersen et al., 2010; Taylor et al., 2000). Recently, Hard AAs have previously been identified within the study area as part of the hydrate system within the shallowest stratigraphic unit across the Exmouth Plateau by Paganoni et al. (2019). Without direct calibration, we are unable to differentiate between these equally plausible alternatives, although we note that the hard AAs all fall within the hydrate stability zone as modelled by Paganoni et al. (2019) (Fig. 7C).

In summary, the leakage zone comprises a ~1 km wide zone emanating from the crestal portion the MS1 reservoir in the underlying Mungaroo Trap. The uppermost part of this zone consists of alternations of soft and hard AAs attributed to the presence of free gas and cemented or diagenetically altered regions for which a gas flux would be a requirement. That the gas flux had multiple points of egress at the modern sea floor as evidenced by the clustered pockmark field located at the top of the leakage zone (Fig. 8).

4.5. Reservoir and leakage volumetric calculations

Based on the interpretation of the DHIs described above, the likely volume of gas that leaked from the MS1 reservoir at the Mungaroo Trap can be calculated. Reservoir properties from the five exploration wells show a significant variation in the net thickness, Net:Gross, water saturation and porosity values of MS1 (Table 3).

Leakage volumes are calculated using a Monte Carlo method with the reservoir property distributions and the areas of the accumulations

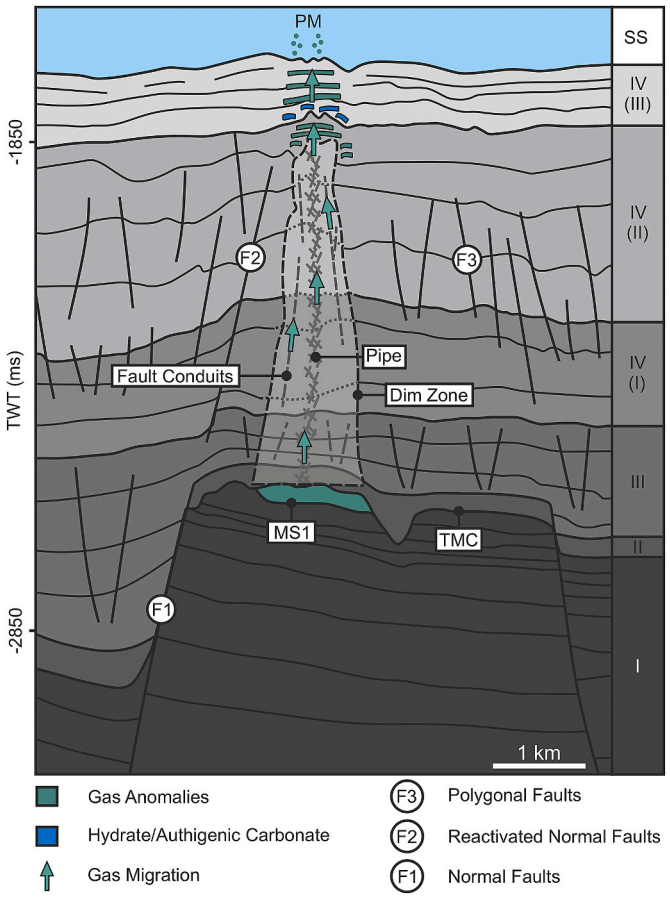

Fig. 8. A schematic cross-section of the hydrocarbon plumbing system displaying the leakage phenomena within Megasequence IV and Fault Systems 1–3. The distribution of pockmarks (PM), gas anomalies and hydrate related leakage phenomena are vertically above the crestal zone of the Mungaroo Trap. The deeper reservoir (MS1) is connected to the shallow subsurface by vertical fluid migration pathways bypassing the Top Mungaroo Claystone (TMC). These are inferred from the dim zone and include fault and pipe conduits. (Colour 1 column). (For interpretation of the references to colour in this figure legend, the reader is referred to the Web version of this article.)

defined by the outline of the trap to the present day and paleo GWCs (see Data and Methods). This allowed leakage volume filled (present-day GWC) and depleted (paleo-GWC) reservoir volumes to be calculated (Fig. 9, Table 4).

Leakage is assumed to have released all original gas in the reservoir down to the position defined by the paleo-GWC. Since depletion is likely to lead to some small fraction of residual gas remaining in the pore space, and at least 1% of residual gas is required to explain the geophysical response of the reservoir in the moderate amplitude region (Brown, 2011), a 100% leakage scenario is unrealistic. However, in the absence of any direct calibration of the depleted reservoir, a null value of residual saturation is used to avoid any arbitrary assignment.

A volumetric difference between the paleo- and present-day gas accumulations is calculated as 0.9 Tcf (see Fig. 9 for range and interquartile range of calculations). The difference between the two GWCs is interpreted as volume lost through leakage from the paleo-GWC volume to the present-day GWC volume. Therefore, the paleo-GWC indicates the leakage from the Mungaroo Trap is at least 0.9 Tcf (Fig. 9, Table 4). However, if there had been complete leakage of the Mungaroo Trap from the position of the paleo-GWC, followed by partial recharge, this would correspond to 1.1 Tcf of leaked gas (Fig. 9, Table 4).

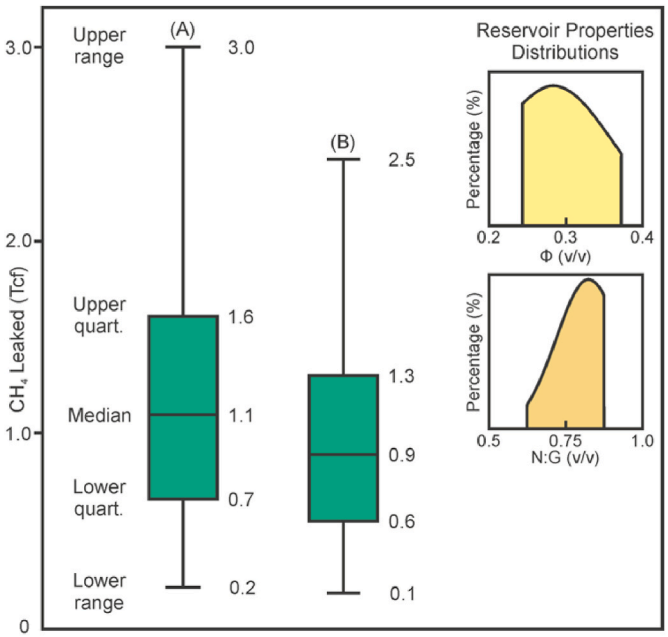

Fig. 9. A box and whisker plot showing the statistical distribution of calculations for two leakage scenarios of the Mungaroo Trap. (A) Complete Leakage from the paleo-GWC (B) Leakage to the current GWC. Includes the distribution of porosity (Φ) and net-to-gross (N:G). (Colour, 1 column). (For interpretation of the references to colour in this figure legend, the reader is referred to the Web version of this article.)

5. Discussion

The interpretation of the present day and paleo GWCs for the MS1 reservoir is consistent with leakage of approximately 1 Tcf from the Mungaroo Trap, which likely depleted the original gas accumulation. The evidence for a crestal failure of the top seal is strongly suggested by the vertical stacking of 'seismic leakage indicators' in the overburden directly above the crest of the trap. The 'seismic leakage indicators' also provide direct evidence of an effective hydrocarbon plumbing system connecting the MS1 reservoir to the seafloor. However, we now need to address a number of key outstanding questions relating to the breaching of this trap, namely, when did the leakage occur, what were the gas migration pathways through the overburden, and what was the mechanism driving seal failure?

5.1. *Timing of leakage*

Two lines of evidence have a direct bearing on the discussion of the timing of the leakage from the MS1 reservoir, namely the presence of a pockmark cluster at the modern sea floor and the discordant geometry of the present day GWC, interpreted as evidence of a dynamic fluid contact.

Dynamic GWCs have previously been attributed to reservoir heterogeneity, slow response to previous leakage events and recent active leakage (Dennis et al., 2005; O'Connor and Swarbrick, 2008; Vejbæk et al., 2005). However, good lateral pressure connectivity has been recorded within the Mungaroo reservoirs across the Carnarvon Basin (Ellis et al., 2009; Taylor, 2012; van der Aa et al., 2013) and high permeabilities have been measured within MS1 top reservoir unit (Table 1) (Allen et al., 2013). These observations suggest that neither facies control or delayed response to leakage due to low permeability can be invoked here to explain the lack of conformance to structure. Instead, we suggest that the dynamic contact most likely results from a leakage event that occurred sufficiently recently for the fluid contact not to have fully re-equilibrated.

Pockmarks at the present-day seafloor are a strong indication of

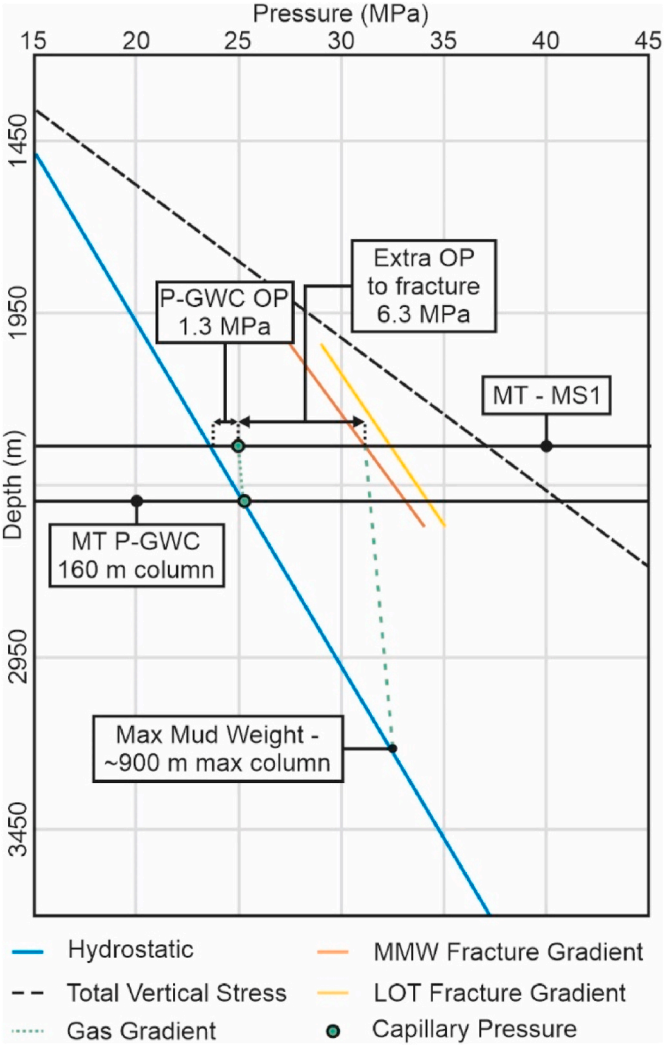

Fig. 10. A pressure depth plot showing the extrapolated fracture gradients, gas gradient, overpressure required for hydraulic fracturing of the top seal, and the subsequent hydraulic seal capacity of the Mungaroo Trap. (Colour, 1 column). (For interpretation of the references to colour in this figure legend, the reader is referred to the Web version of this article.)

Table 4
Summary of median reservoir volumetric values. See Fig. 7 for range and interquartile range of the HC Volume calculations.

GWC	Area (10^6 m^2)	Gross Volume (10^6 m^3)	Net Volume (10^6 m^3)	HC Volume (10^6 m^3)	HC Volume (Tcf)
Paleo	27	740	550	130	1.1
Present-day	5	140	100	20	0.2
CH4 Lost				110	0.9

recent high focused fluid flow sufficient to excavate and remove near surface sediment (Hovland and Judd, 1988). Since the pockmark cluster directly overlies the leakage zone (Fig. 7) we assume that the timing of pockmark formation most likely corresponds to the timing of active gas flux within the leakage zone. Dating the formation of the pockmarks in the study is complicated as there is no direct calibration of the near surface sediments at the Mungaroo Trap. The nearest calibration well is ODP Site 762 where the sea floor is an erosional surface and the near surface sediments are dated at 290 ka (Haq et al., 1990), so based on this we can only provide a crude constraint on the age of the pockmarks as post-dating this erosion surface, i.e., they probably formed at some time in the last 290 ka. By linking the formation of the pockmark cluster to the development of the leakage zone beneath, we therefore suggest that the main leakage event occurred at sometime within the last 290 ka.

6. Mechanisms for leakage

Before determining the mechanisms for leakage, we must first establish the migration mechanisms from the reservoir to the near surface. From the observations of the seismic data, it is difficult to determine if the dim zone represents fluid migration through exploitation of the pre-existing permeability and fracture networks (Sibson, 1994) or through focused fluid flow such as pipes (Hustoft et al., 2010). Both fracture networks (Alrefaee et al., 2018; Dirnstein et al., 2013; Gartrell et al., 2003) and pipe structures (Mercado Ruge et al., 2020) have been shown to be effective fluid migration pathways within the Northern Carnarvon Basin and wider NWS.

'Wipe-out' or 'blanking zones' that display a similar acoustic character to the dim zone described in this study have previously been interpreted as evidence of vertical fluid migration exploiting the pre-existing permeability and fracture network (Bertoni et al., 2018; Heggland, 1997; Judd and Hovland, 1992; Karstens and Berndt, 2015). The loss of signal strength within the dim zone is consistent with multiple, vertically stacked gas charged layers in seismic chimneys (Cathles et al., 2010; Hovland and Judd, 1988). However, focused fluid flow structures have been identified as vertical zones with 'up bent' or 'pull-up' reflections (Gay et al., 2012; Hustoft et al., 2007), and have also been associated with pipes feeding high amplitude anomalies attributed to hydrates (Petersen et al., 2010), like those observed at the top of the dim zone in this study (Fig. 7C). The reduction in image quality within the dim zones makes it difficult to fully assess the precise flow pathways, but the close spatial association of all the leakage indicators is consistent with previous interpretations of similar phenomena as being linked to highly focused vertical gas migration.

The distribution of the leakage zone above the crestal position of Mungaroo Trap (Fig. 7) suggests that leakage has occurred by breaching of the top seal, at or close to the erosional pinch out of the reservoir. However, the precise location or zone of breaching is difficult to identify as there are no leakage indicators within the immediate top seal interval above the MS1 reservoir unit (Fig. 7B). Since the crestal region is sub horizontal (Fig. 6), similar conditions of pressure and phase would be expected over a limited area. The pinch out position is located ~1 km up flank from the position of Fault X (Fig. 5), therefore it is unlikely that leakage can be attributed to breach of a fault seal. Leakage at the crestal position is more indicative of a pressure control and is instead more plausibly attributed to capillary or hydraulic seal failure (Sales, 1997; Watts, 1987).

Although, as argued above hydraulic seal failure is the most plausible means to explain highly focused fluid flow across c. 1000 m of generally fine-grained overburden sediments, some element of slow seepage from the Mungaroo Trap through capillary invasion cannot be discounted. Pockmarks at the present-day seafloor are usually attributed to higher flux focused fluid flow rather than low flux seepage (Cartwright et al., 2007). However, this could also be achieved through slow seepage at depth before shallow storage of gas within the GHSZ before venting to the seafloor (Andreassen et al., 2017). On balance however, it is noteworthy that the immediate Top Mungaroo Claystone (TMC) top seal has been shown to be highly effective regionally in the basin, with gas discoveries at Arnhem, Brederode and Eendracht, none of which display evidence of top seal breach (Allen et al., 2013; Mahon and Ellis, 2011; Twartz, 1981). Elsewhere on the Exmouth Plateau, column heights of up to 500 m have been recorded within Mungaroo reservoirs (Jablonski et al., 2013). This is significantly larger than the column height down to the paleo-GWC identified within the Mungaroo Trap. There is no seismic evidence of leakage within the immediate TMC top seal or overlying Athol Formation or Barrow Group sealing units and a dynamic GWC

indicates a higher rate of flux, and hence we suggest that capillary leakage is unlikely to have been a major factor in the entire leakage process.

Previous studies have documented leakage events within the Carnarvon Basin and across the North West Shelf and have invoked a diversity of mechanisms involving for example, hydraulic fracturing (Foschi and Cartwright, 2020), or leakage along fault planes and fracture systems (Bailey et al., 2006; Gartrell et al., 2003). Both represent a subset of the more general mechanism of hydraulic seal failure which occurs when the reservoir pressure is large enough to intersect the fracture gradient (Watts, 1987). Extrapolation of the mud weight fracture gradient from Arnhem-1 to the depth of the Mungaroo Trap (See Data and Methods) shows that to initiate hydraulic fracturing of the top seal 7.6 MPa of overpressure is required (Fig. 10). This is the equivalent to a buoyancy force exerted by a ~900 m gas column given a methane density of 170 kg m^{-3}. Since the paleo-GWC of the top reservoir only shows evidence for a 160 m gas column height (equivalent to 1.3 MPa overpressure, Fig. 10), this implies that a 6.3 MPa increase in aquifer pressure would have been required in order to induce hydraulic fracturing of the top seal. The processes that may be considered plausible to achieve these pressure increases are discussed in the following section.

6.1. Overpressure generation

To initiate hydraulic seal failure, a substantial increase in aquifer pressure needs to be induced or less likely, an increase in fracture pressure derived from a substantially larger gas column. The only way to achieve a much larger gas column would be by communication between vertically stacked gas filled reservoir sands. This is not the case at the present day at Arnhem-1, where formation pressure data show the reservoirs have individual gas gradients, showing that they are not in pressure communication (Allen et al., 2013). It is conceivable that a vertical communication route could have been opened between the deeper reservoirs at the Mungaroo Trap. This could be achieved by reactivation or dilation of the major fault (Fault X – Fig. 7) or the antithetic faults connecting the vertically stacked reservoirs, such as pressure valving along faults as proposed by Sibson (1994), or direct vertical transfer of pressure along dilated fault planes by Grauls and Baleix (1994). Pockmark craters are observed on the top reservoir horizon MS1 (Fig. 5A) and have been linked to fluid migration through fault flow (Velayatham et al., 2018) or through vertical fracture systems formed by emplacement of magmatic dykes (Magee and Jackson, 2020; Velayatham, 2019). Both mechanisms would create the necessary vertical permeable pathways that could be exploited by later stresses to cause reactivation or dilation and increase permeability.

Aquifer overpressure within Mungaroo reservoirs has been observed within the Northern Carnarvon Basin (Tingate et al., 2001; van Ruth et al., 2004). However, these are within isolated compartments, with the basin generally having good lateral hydraulic connectivity (Otto et al., 2001). The aquifer at Arnhem-1 is hydrostatically pressured at the present day (Fig. 3) (Allen et al., 2013). Due to their proximity, it is assumed that the Arnhem discovery and Mungaroo Trap are within a connected aquifer. Within this aquifer system the Arnhem discovery is found down-dip of the Mungaroo Trap, allowing Arnhem to behave as a protected trap (Winefield et al., 2005). Any increases in aquifer overpressure would be focused within the shallower Mungaroo Trap making this the leak point of the system leaving the Arnhem discovery protected from leakage (e.g., Winefield et al., 2005).

Borehole breakout data and doming of the present-day seafloor suggests that the maximum horizontal stress is orientated ESE-WNW, consistent with inversion structures and anticlines formed through the Neogene (Hillis et al., 2008). The present-day stress field would be capable of dilating or reactivating the preferentially aligned fault and fractures networks within the reservoir or increasing aquifer pressure through compression.

In summary, the precise mechanisms responsible for leakage at the Mungaroo Trap and other localities across the Northern Carnarvon Basin and North West Shelf remain an open research question. Under the present-day stress regime both fault flow and classical top seal hydraulic leakage are valid mechanisms for leakage of the Mungaroo Trap. In this instance, due to a well-defined leakage zone above the crestal zone of the trap offset from the fault plane, hydraulic failure is the preferred mechanism for top seal breach, but with uncertainty over the precise mechanism necessary to generate the required pressure conditions for seal failure.

7. Conclusions

Mapping of seismic and well data from the Exmouth Plateau, North West Shelf of Australia has allowed for the characterization of the Mungaroo Trap and the associated leakage zone. It is recognised here as an example of a combination structural-stratigraphic trap that has experienced significant leakage through top seal failure and where leaked gas migrated through the immediate top seal to the shallow subsurface through focused fluid flow pathways.

The Mungaroo Trap has undergone significant leakage of at least 0.9 Tcf sourced from the deep Triassic aged reservoirs. This is a recent leakage event having occurred in the last 300 ka.

Leakage has occurred through breach of the top seal at the crestal zone of the top reservoir unit, attributed to hydraulic failure of the top seal. This process was possibly driven by hard overpressure generated by an increased gas column or reservoir aquifer pressure.

This study demonstrates how the outlined methodology, integrating well and seismic interpretation of both paleo- and present-day GWCs, can be successfully used to calculate the leaked volume of a hydrocarbon trap. This methodology can be applied to future study areas to understand the severity of top seal breach in both hydrocarbon and subsurface carbon sequestration reservoirs to improve de-risking assessments.

The results indicate that hydrocarbon reservoirs are capable of leaking significant volumes of methane within a relatively geologically instantaneous period. The Mungaroo Trap and Exmouth Plateau have been shown to be part of a wider leaking hydrocarbon province on Australia's North West Shelf. Further work is required to investigate what is driving regional leakage across the NWS and to understand if this is part of a larger scale, regionally synchronous event.

Declaration of competing interest

The authors declare that they have no known competing financial interests or personal relationships that could have appeared to influence the work reported in this paper.

Data availability

All data available from Australian National Offshore Petroleum Information Management System (NOPIMS)

Acknowledgements

University of Oxford Clarendon Fund Jesus College Oxford and Oxford DTP in Environmental Research are thanked for funding. We would like to thank Schlumberger for providing a Petrel license. Seismic and well data were supplied by Geoscience Australia through access to the National Offshore Petroleum Information Management System (NOPIMS). We thank C. Kirkham for their helpful discussion.

References

Abrams, M.A., 1992. Geophysical and geochemical evidence for subsurface hydrocarbon leakage in the Bering Sea, Alaska. Mar. Petrol. Geol. 9, 208–221. https://doi.org/10.1016/0264-8172(92)90092-S.

Allen, P., van der Aa, D., Rodger, S., 2013. Arnhem-1 Final Well Completion Report Carnarvon Basin. WA-364-P (R1).

Alrefaee, H.A., Gosh, S., Abdel-Fattah, M.I., 2018. 3D seismic characterization of the polygonal fault systems and its impact on fluid flow migration: an example from the Northern Carnarvon Basin, Australia. J. Pet. Sci. Eng. 167, 120–130. https://doi.org/10.1016/j.petrol.2018.04.009.

Andreassen, K., Hubbard, A., Winsborrow, M., Patton, H., Vadakkepuliyambatta, S., Plaza-Faverola, A., Gudlaugsson, E., Serov, P., Deryabin, A., Mattingsdal, R., Mienert, J., Bünz, S., 2017. Massive blow-out craters formed by hydrate-controlled methane expulsion from the Arctic seafloor. Science 356, 948–953. https://doi.org/10.1126/science.aal4500, 1979.

Andresen, K.J., 2012. Fluid flow features in hydrocarbon plumbing systems: what do they tell us about the basin evolution? Mar Geol 332– 334, 89–108. https://doi.org/10.1016/j.margeo.2012.07.006.

Bailey, W.R., Underschultz, J., Dewhurst, D.N., Kovack, G., Mildren, S., Raven, M., 2006. Multi-disciplinary approach to fault and top seal appraisal; Pyrenees-Macedon oil and gas fields, Exmouth Sub-basin, Australian Northwest Shelf. Mar. Petrol. Geol. https://doi.org/10.1016/j.marpetgeo.2005.08.004.

Barber, P.M., 1982. Palaeotectonic evolution and hydrocarbon genesis of the central Exmouth Plateau. The APPEA Journal 22, 131–144.

Berndt, C., Costa, S., Canals, M., Camerlenghi, A., de Mol, B., Saunders, M., 2012. Repeated slope failure linked to fluid migration: the Ana submarine landslide complex, Eivissa Channel, Western Mediterranean Sea. Earth Planet Sci. Lett. 319, 65–74.

Bertoni, C., Cartwright, J., Foschi, M., Martin, J., 2018. Spectrum of gas migration phenomena across multilayered sealing sequences. Am. Assoc. Petrol. Geol. Bull. 102, 1011–1034. https://doi.org/10.1306/0810171622617210.

Bilal, A., McClay, K., 2022. Tectonic and stratigraphic evolution of the central Exmouth Plateau, NW shelf of Australia. Mar. Petrol. Geol. 136, 105447 https://doi.org/10.1016/j.marpetgeo.2021.105447.

Bilal, A., McClay, K., Scarselli, N., 2020. Fault-scarp degradation in the central exmouth plateau, north west shelf, Australia. Geol. Soc. Spec. Publ. 476, 231–257. https://doi.org/10.1144/SP476.11.

Boyd, R., Williamson, P., Haq, B., 1992. Seismic stratigraphy and passive margin evolution of the southern Exmouth Plateau. Proc. scientific results, ODP, Leg 122, Exmouth Plateau 122, 39–59. https://doi.org/10.2973/odp.proc.sr.122.122.1992.

Brincat, M., Gartrell, A., Lisk, M., Bailey, W., Johnson, L., Dewhurst, D., 2006. An integrated evaluation of hydrocarbon charge and retention at the Griffin, Chinook, and Scindian oil and gas fields, Barrow Subbasin, North West Shelf, Australia. AAPG (Am. Assoc. Pet. Geol.) Bull. 90, 1359–1380. https://doi.org/10.1306/02210605103.

Brown, A.R., 2011. Interpretation of Three-Dimensional Seismic Data. Society of Exploration Geophysicists and American Association of Petroleum Geologists. https://doi.org/10.1190/1.9781560802884.

Bünz, S., Mienert, J., 2004. Acoustic imaging of gas hydrate and free gas at the Storegga slide. J. Geophys. Res. Solid Earth 109, 1–15. https://doi.org/10.1029/2003JB002863.

Bussell, M.R., Jablonski, D., Enman, T., Wilson, M.J., Bint, A.N., 2001. Deepwater exploration: north western Australia compared with gulf of Mexico and Mauritania. The APPEA Journal 41, 289. https://doi.org/10.1071/aj00014.

Cartwright, J., Huuse, M., Aplin, A., 2007. Seal bypass systems. Am. Assoc. Petrol. Geol. Bull. 91, 1141–1166. https://doi.org/10.1306/04090705181.

Cathles, L.M., Su, Z., Chen, D., 2010. The physics of gas chimney and pockmark formation, with implications for assessment of seafloor hazards and gas sequestration. Mar. Petrol. Geol. 27, 82–91. https://doi.org/10.1016/j.marpetgeo.2009.09.010.

Chiaramonte, L., Zoback, M.D., Friedmann, J., Stamp, V., 2008. Seal integrity and feasibility of CO2 sequestration in the Teapot Dome EOR pilot: geomechanical site characterization. Environ. Geol. 54, 1667–1675. https://doi.org/10.1007/s00254-007-0948-7.

Chongzhi, T., Guoping, B., Junlan, L., Chao, D., Xiaoxin, L., Houwu, L., Dapeng, W., Yuan, W., Min, L., 2013. Mesozoic lithofacies palaeogeography and petroleum prospectivity in North Carnarvon Basin, Australia. J. Palaeogeogr. 2, 81–92. https://doi.org/10.3724/SP.J.1261.2013.00019.

Cook, A.C., Smyth, M., Vos, R.G., 1985. Source potential of upper triassic fluvio-deltaic systems of the Exmouth Plateau. The APPEA Journal 25, 204–215.

Cowley, R., O'Brien, G.W., 2000. Identification and interpretation of leaking hydrocarbons using seismic data: a comparative montage of examples from the major fields in Australia's Northwest Shelf and Gippsland Basin. The APPEA Journal 40, 119. https://doi.org/10.1071/AJ99008.

Cox, D.R., Huuse, M., Newton, A.M.W., Sarkar, A.D., Knutz, P.C., 2021. Shallow gas and gas hydrate occurrences on the northwest Greenland shelf margin. Mar. Geol. 432, 106382 https://doi.org/10.1016/j.margeo.2020.106382.

Cox, D.R., Newton, A.M.W., Huuse, M., 2020. An introduction to seismic reflection data: acquisition, processing and interpretation. In: Regional Geology and Tectonics: Principles of Geologic Analysis Volume 1: Principles of Geologic Analysis. Elsevier, pp. 571–603. https://doi.org/10.1016/B978-0-444-64134-2.00020-1.

Dennis, H., Bergmo, P., Holt, T., 2005. Tilted oil–water contacts: modelling the effects of aquifer heterogeneity. Geological Society, London, Petroleum Geology Conference series 6, 145–158. https://doi.org/10.1144/0060145.

Dewhurst, D.N., Hennig, A.L., 2003. Geomechanical properties related to top seal leakage in the Carnarvon Basin, Northwest Shelf, Australia. Petrol. Geosci. 9, 255–263. https://doi.org/10.1144/1354-079302-557.

Dewhurst, D.N., Jones, R.M., Raven, M.D., 2002. Microstructural and petrophysical characterization of Muderong Shale: application to top seal risking. Petrol. Geosci. 8, 371–383. https://doi.org/10.1144/petgeo.8.4.371.

Dirnstein, J.K., Hengesh, J. v, Stanley, A.J., 2013. Identification of fluid flow features in the seafloor and subsurface and their implications for prospect and geohazard assessment: examples from the Australian northwest shelf. Western Australian Basins Symposium 1–21.

Donovan, T.J., 1974. Petroleum microseepage at cement, Oklahoma: evidence and mechanism. Am. Assoc. Petrol. Geol. Bull. 58, 429–446. https://doi.org/10.1306/83D9140C-16C7-11D7-8645000102C1865D.

Downey, M.W., 1984. Evaluating seals for hydrocarbon accumulations. Am. Assoc. Petrol. Geol. Bull. 68, 1752–1763.

Ellis, C., Woodall, M., Lim, D., 2009. Thebe-2 and Thebe-2CH Well Completion Report Interpretive, ume. WA-346-P.

Exon, N.F., Buffler, R.T., 1992. Mesozoic seismic stratigraphy and tectonic evolution of the western Exmouth Plateau. Proc. scientific results, ODP, Leg 122, Exmouth Plateau 122, 61–81. https://doi.org/10.2973/odp.proc.sr.122.125.1992.

Exon, N.F., von Rad, U., von Stackelberg, U., 1982. The geological development of the passive margins of the Exmouth Plateau off northwest Australia. Mar. Geol. 47, 131–152. https://doi.org/10.1016/0025-3227(82)90023-8.

Exon, N.F., Willcox, J.B., 1978. Geology and petroleum potential of Exmouth Plateau area off western Australia. AAPG Bull. 62, 40–72. https://doi.org/10.1306/c1ea47f2-16c9-11d7-8645000102c1865d.

Exon, N.P., Haq, B.U., von Rad, U., 1992. Exmouth Plateau revisited: scientific drilling and geological framework. In: Proceedings of the Ocean Drilling Program, 122 Scientific Results. Ocean Drilling Program. https://doi.org/10.2973/odp.proc.sr.122.194.1992.

Fischer, D., Mogollón, J.M., Strasser, M., Pape, T., Bohrmann, G., Fekete, N., Spiess, V., Kasten, S., 2013. Subduction zone earthquake as potential trigger of submarine hydrocarbon seepage. Nat. Geosci. 6, 647–651. https://doi.org/10.1038/ngeo1886.

Foschi, M., Cartwright, J.A., 2020. Seal failure assessment of a major gas field via integration of seal properties and leakage phenomena. Am. Assoc. Petrol. Geol. Bull. 104, 1627–1648. https://doi.org/10.1306/02282018111.

Foschi, M., Cartwright, J.A., Peel, F.J., 2014. Vertical anomaly clusters: evidence for vertical gas migration across multilayered sealing sequences. Am. Assoc. Petrol. Geol. Bull. 98, 1859–1884. https://doi.org/10.1306/04051413121.

Foschi, M., MacMinn, C.W., Etiope, G., 2020. Evidence for massive emission of methane from a deep-water gas field during the Pliocene. Proc. Natl. Acad. Sci. U. S. A. 117, 27869–27876. https://doi.org/10.1073/pnas.2001904117.

Gartrell, A., Yanhua, Z., Lisk, M., Dewhurst, D., 2003. Enhanced hydrocarbon leakage at fault intersections: an example from the Timor Sea, Northwest Shelf, Australia. J. Geochem. Explor. 78–79, 361–365. https://doi.org/10.1016/S0375-6742(03)00125-0.

Gartrell, A., Zhang, Y., Lisk, M., Dewhurst, D., 2004. Fault intersections as critical hydrocarbon leakage zones: integrated field study and numerical modelling of an example from the Timor Sea, Australia. Mar. Petrol. Geol. 21, 1165–1179. https://doi.org/10.1016/j.marpetgeo.2004.08.001.

Gay, A., Lopez, M., Cochonat, P., Séranne, M., Levaché, D., Sermondadaz, G., 2006. Isolated seafloor pockmarks linked to BSRs, fluid chimneys, polygonal faults and stacked Oligocene–Miocene turbiditic palaeochannels in the Lower Congo Basin. Mar. Geol. 226, 25–40. https://doi.org/10.1016/j.margeo.2005.09.018.

Gay, A., Mourgues, R., Berndt, C., Bureau, D., Planke, S., Laurent, D., Gautier, S., Lauer, C., Loggia, D., 2012. Anatomy of a fluid pipe in the Norway Basin: initiation, propagation and 3D shape. Mar Geol 332– 334, 75–88. https://doi.org/10.1016/j.margeo.2012.08.010.

Geoscience Australia, 2020. Regional Geology of the Northern Carnarvon Basin.

Grauls, D.J., Baleix, J.M., 1994. Role of overpressures and in situ stresses in fault-controlled hydrocarbon migration: a case study. Mar. Petrol. Geol. 11, 734–742. https://doi.org/10.1016/0264-8172(94)90026-4.

Gutierrez, M.A., 2022. Rock physics-based characterization of tertiary hydrocarbon migration: seismic de-risking of false positive DHIs related to residual gas. In: Second International Meeting for Applied Geoscience & Energy. Society of Exploration Geophysicists and American Association of Petroleum Geologists, pp. 2298–2302. https://doi.org/10.1190/image2022-3751929.1.

Haq, B.U., Boyd, R.L., Exon, N.F., von Rad, U., 1992. Evolution of the central Exmouth Plateau: a post-drilling perspective. Proc. scientific results, ODP, Leg 122, Exmouth Plateau 122, 801–816. https://doi.org/10.2973/odp.proc.sr.122.182.1992.

Haq, B.U., von Rad, U., O'Connell, S., et al., 1990. Site 762. In: Proceedings of the Ocean Drilling Program, 122 Initial Reports. Ocean Drilling Program, pp. 301–343. https://doi.org/10.2973/odp.proc.ir.122.108.1990.

Heggland, R., 2005. Using gas chimneys in seal integrity analysis: a discussion based on case histories. In: Boult, P., Kaldi, J. (Eds.), Evaluating Fault and Cap Rock Seals. AAPG Special Volumes, Tulsa. https://doi.org/10.1306/1060767H23170.

Heggland, R., 1998. Gas seepage as an indicator of deeper prospective reservoirs. A study based on exploration 3D seismic data. Mar. Petrol. Geol. 15, 1–9. https://doi.org/10.1016/S0264-8172(97)00060-3.

Heggland, R., 1997. Detection of gas migration from a deep source by the use of exploration 3D seismic data. Mar. Geol. 137, 41–47. https://doi.org/10.1016/S0025-3227(96)00077-1.

Hermanrud, C., Bolås, H.M.N., 2002. Leakage from Overpressured Hydrocarbon Reservoirs at Haltenbanken and in the Northern North Sea, pp. 221–231. https://doi.org/10.1016/S0928-8937(02)80017-0.

Hillis, R.R., Sandiford, M., Reynolds, S.D., Quigley, M.C., 2008. Present-day stresses, seismicity and Neogene-to-Recent tectonics of Australia's "passive" margins: intraplate deformation controlled by plate boundary forces. Geol. Soc. Spec. Publ. 306, 71–90. https://doi.org/10.1144/SP306.3.

Hovland, M., Judd, A.G., 1988. Seabed Pockmarks and Seepages : Impact on Geology, Biology, and the Marine Environment. Graham & Trotman, London. https://doi.org/10.13140/RG.2.1.1414.1286.

Hustoft, S., Bünz, S., Mienert, J., 2010. Three-dimensional seismic analysis of the morphology and spatial distribution of chimneys beneath the Nyegga pockmark

field, offshore mid-Norway. Basin Res. 22, 465–480. https://doi.org/10.1111/j.1365-2117.2010.00486.x.
Hustoft, S., Mienert, J., Bünz, S., Nouzé, H., 2007. High-resolution 3D-seismic data indicate focused fluid migration pathways above polygonal fault systems of the mid-Norwegian margin. Mar. Geol. 245, 89–106. https://doi.org/10.1016/j.margeo.2007.07.004.
Imbert, P., Ho, S., 2012. Seismic-scale funnel-shaped collapse features from the paleocene-eocene of the North West West Shelf of Australia. Mar. Geol. 332–334, 198–221. https://doi.org/10.1016/j.margeo.2012.10.010.
Ingram, G.M., Urai, J.L., 1999. Top-seal leakage through faults and fractures: the role of mudrock properties. Geological Society, London, Special Publications 158, 125–135. https://doi.org/10.1144/GSL.SP.1999.158.01.10.
Jablonski, D., Preston, J., Westlake, S., Gumley, C.M., 2013. Unlocking the origin of hydrocarbons in the central part of the Rankin trend, northern Carnarvon Basin, Australia. In: The Sedimentary Basins of Western Australia IV. Proceedings of the Petroleum Exploration Society of Australia Symposium, Perth, Australia, pp. 1–31.
Jahn, F., Cook, M., Graham, M., 2008. Hydrocarbon exploration and production. In: Developments in Petroleum Science, second ed. Elsevier, Amsterdam.
Judd, A., Hovland, M., 2007. Seabed Fluid Flow-Impact of Geology, Biology and the Marine Environment. Cambridge University Press, Cambridge. https://doi.org/10.1017/CBO9780511535918. Cambridge University Press.
Judd, A.G., Hovland, M., 1992. The evidence of shallow gas in marine sediments. Continent. Shelf Res. 12, 1081–1095. https://doi.org/10.1016/0278-4343(92)90070-Z.
Karstens, J., Berndt, C., 2015. Seismic chimneys in the Southern Viking Graben - implications for palaeo fluid migration and overpressure evolution. Earth Planet Sci. Lett. 412, 88–100. https://doi.org/10.1016/j.epsl.2014.12.017.
Keep, M., Harrowfield, M., Crowe, W., 2007. The Neogene tectonic history of the North West West Shelf, Australia. Explor. Geophys. 38, 151–174. https://doi.org/10.1071/EG07022.
Kennicutt, M.C., Brooks, J.M., Bidigare, R.R., Fay, R.R., Wade, T.L., McDonald, T.J., 1985. Vent-type taxa in a hydrocarbon seep region on the Louisiana slope. Nature 317, 351–353. https://doi.org/10.1038/317351a0.
Kovack, G.E., Dewhurst, D.N., Raven, M.D., Kaldi, J.G., 2004. The influence of composition, diagenesis and compaction on seal capacity in the Muderong shale, Carnarvon Basin. The APPEA Journal 44, 201. https://doi.org/10.1071/aj03007.
Krooss, B.M., Leythaeuser, D., Schaefer, R.G., 1992. The quantification of diffusive hydrocarbon losses through cap rocks of natural gas reservoirs - a reevaluation. Am. Assoc. Petrol. Geol. Bull. 76 https://doi.org/10.1306/BDFF881C-1718-11D7-8645000102C1865D.
Ligtenberg, J.H., 2005. Detection of Fluid migration pathways in seismic data: implications for fault seal analysis. Basin Res. 17, 141–153. https://doi.org/10.1111/j.1365-2117.2005.00258.x.
Lisk, M., O'brien, G.W., Eadington, P.J., 2002. Quantitative Evaluation of the Oil-Leg Potential in the Oliver Gas Field, Timor Sea, Australia, vol. 86. AAPG Bulletin.
Longley, I.M., Buessenschuett, C., Clydsdale, L., Cubitt, C.J., Davis, R.C., Johnson, M.K., Marshall, N.M., Murray, A.P., Somerville, R., Spry, T.B., 2002. The north west shelf of Australia—a Woodside perspective. In: The Sedimentary Basins of Western Australia 3: Proceedings of the Petroleum Exploration Society of Australia Symposium, Perth. Pet. Explor. Soc. of Aust. Perth, pp. 27–88.
Løseth, H., Gading, M., Wensaas, L., 2009. Hydrocarbon leakage interpreted on seismic data. Mar. Petrol. Geol. 26, 1304–1319. https://doi.org/10.1016/j.marpetgeo.2008.09.008.
Løseth, H., Wensaas, L., Arntsen, B., Hanken, N.M., Basire, C., Graue, K., 2011. 1000 M long gas blow-out pipes. Mar. Petrol. Geol. 28, 1040–1060. https://doi.org/10.1016/j.marpetgeo.2010.10.001.
Magee, C., Duffy, O.B., Purnell, K., Bell, R.E., Jackson, C.A.L., Reeve, M.T., 2016. Fault-controlled fluid flow inferred from hydrothermal vents imaged in 3D seismic reflection data, offshore NW Australia. Basin Res. 28, 299–318. https://doi.org/10.1111/bre.12111.
Magee, C., Jackson, C. al, 2020. Seismic reflection data reveal the 3D structure of the newly discovered Exmouth Dyke Swarm, offshore NW Australia. Solid Earth 11, 579–606. https://doi.org/10.5194/se-11-579-2020.
Mahon, E., Ellis, C., 2011. Brederode 1 Carnarvon Basin: WA-364-P (R1) Well Completion Report.
Mathieu, C.J.H., 2018. Exploration well failures from the UK North sea. Petroleum Geology Conference Proceedings 8, 267–272. https://doi.org/10.1144/PGC8.3.
Medouri, G., Ramsingh, R., Gomez, C., Oviedo, J., Roncero, L., 2015. Paleo Residual Gas in Columbus Basin: Examples from TSP Oil/gas Field.
Mercado Ruge, S., Scarselli, N., Bilal, A., 2020. 3D seismic classification of fluid escape pipes in the western Exmouth Plateau, North West Shelf of Australia (A). J Geol Soc London. https://doi.org/10.1144/jgs2020-096 jgs2020-096.
Milkov, A.v., Samis, J.M., 2020. Turning dry holes from disasters to exploration wisdom: decision tree to determine the key failure mode for segments in conventional petroleum prospects. Am. Assoc. Petrol. Geol. Bull. 104, 449–475. https://doi.org/10.1306/05061918229.
Müller, R.D., Dyksterhuis, S., Rey, P., 2012. Australian paleo-stress fields and tectonic reactivation over the past 100 Ma. Aust. J. Earth Sci. 59, 13–28. https://doi.org/10.1080/08120099.2011.605801.
Nugraha, H.D., Jackson, C.A.L., Johnson, H.D., Hodgson, D.M., Reeve, M.T., 2019. Tectonic and oceanographic process interactions archived in Late Cretaceous to Present deep-marine stratigraphy on the Exmouth Plateau, offshore NW Australia. Basin Res. 31, 405–430. https://doi.org/10.1111/bre.12328.
O'Brien, G.W., Cowley, R., Lawrence, G., Williams, A.K., Webster, M., Tingate, P., Burns, S., 2003. Migration, leakage and seepage characteristics of the offshore Canning Casin and Northern Carnarvon basin: implications for hydrocarbon prospectivity. The APPEA Journal 43, 149. https://doi.org/10.1071/AJ02072.
O'Brien, G.W., Lawrence, G.M., Williams, A.K., Glenn, K., Barrett, A.G., Lech, M., Edwards, D.S., Cowley, R., Boreham, C.J., Summons, R.E., 2005. Yampi Shelf, Browse Basin, North-West Shelf, Australia: a test-bed for constraining hydrocarbon migration and seepage rates using combinations of 2D and 3D seismic data and multiple, independent remote sensing technologies. Mar. Petrol. Geol. 22, 517–549. https://doi.org/10.1016/j.marpetgeo.2004.10.027.
O'Brien, G.W., Woods, E.P., 1995. Hydrocarbon-related diagenetic zones (HRDZs) in the Vulcan Sub-basin, Timor Sea: recognition and exploration implications. The APPEA Journal 35, 220. https://doi.org/10.1071/AJ94015.
O'Connor, S.A., Swarbrick, R.E., 2008. Pressure regression, fluid drainage and a hydrodynamically controlled fluid contact in the North sea, lower cretaceous, britannia sandstone formation. Petrol. Geosci. 14, 115–126. https://doi.org/10.1144/1354-079308-737.
Ostanin, I., Anka, Z., di Primio, R., 2017. Role of faults in hydrocarbon leakage in the hammerfest basin, SW barents sea: insights from seismic data and numerical modelling. Geosciences 7. https://doi.org/10.3390/geosciences7020028.
Otto, C.J., Underschultz, J.R., Hennig, A.L., Roy, V.J., 2001. Hydrodynamic analysis of flow systems and Fault seal integrity in the North West West Shelf of Australia. The APPEA Journal 41, 347. https://doi.org/10.1071/aj00016.
Paganoni, M., King, J.J., Foschi, M., Mellor-Jones, K., Cartwright, J.A., 2019. A natural gas hydrate system on the Exmouth Plateau (NW shelf of Australia) sourced by thermogenic hydrocarbon leakage. Mar. Petrol. Geol. 99, 370–392. https://doi.org/10.1016/j.marpetgeo.2018.10.029.
Petersen, C.J., Bünz, S., Hustoft, S., Mienert, J., Klaeschen, D., 2010. High-resolution P-Cable 3D seismic imaging of gas chimney structures in gas hydrated sediments of an Arctic sediment drift. Mar. Petrol. Geol. 27, 1981–1994. https://doi.org/10.1016/j.marpetgeo.2010.06.006.
Rahman, M.J., Fawad, M., Jahren, J., Mondol, N.H., 2022. Top seal assessment of Drake Formation shales for CO2 storage in the Horda Platform area, offshore Norway. Int. J. Greenh. Gas Control 119. https://doi.org/10.1016/j.ijggc.2022.103700.
Räss, L., Simon, N.S.C., Podladchikov, Y.Y., 2018. Spontaneous formation of fluid escape pipes from subsurface reservoirs. Sci. Rep. 8 https://doi.org/10.1038/s41598-018-29485-5.
Riera, R., Paumard, V., de Gail, M., Saqab, M.M., Lebrec, U., Lang, S.C., Lane, A., 2022. Origin of seafloor pockmarks overlying submarine landslides: insights from semi-automated mapping of 3D seismic horizons (North West Shelf, Australia). Mar. Petrol. Geol. 136 https://doi.org/10.1016/j.marpetgeo.2021.105453.
Roberts, H.H., Carney, R.S., 1997. Evidence of episodic fluid, gas, and sediment venting on the northern Gulf of Mexico continental slope. Econ. Geol. 92, 863–879. https://doi.org/10.2113/gsecongeo.92.7-8.863.
Rollet, N., Logan, G.A., Kennard, J.M., O'Brien, P.E., Jones, A.T., Sexton, M., 2006. Characterisation and correlation of active hydrocarbon seepage using geophysical data sets: an example from the tropical, carbonate Yampi Shelf, Northwest Australia. Mar. Petrol. Geol. 23, 145–164. https://doi.org/10.1016/j.marpetgeo.2005.10.002.
Rudolph, K.W., Goulding, F.J., 2017. Benchmarking exploration predictions and performance using 20+ yr of drilling results: one company's experience. Am. Assoc. Petrol. Geol. Bull. 101, 161–176. https://doi.org/10.1306/06281616060.
Sales, J.K., 1997. Seal strength vs. Trap closure–A fundamental control on the distribution of oil and gas. In: Surdam, R.C. (Ed.), Seals, Traps, and the Petroleum System. American Association of Petroleum Geologists. https://doi.org/10.1306/M67611C5.
Sassen, R., Losh, S.L., Iii, L.C., Roberts, H.H., Whelan, J.K., Milkov, A. v, 2001. Massive vein- ® lling gas hydrate : relation to ongoing gas migration from the deep subsurface in the. Gulf of Mexico 18, 551–560.
Scarselli, N., Elders, C., 2013. Submarine slide and slump complexes, Exmouth Plateau, NW shelf of Australia. The Sedimentary Basin of Western Australia IV 4, 1–19.
Schroot, B.M., Schüttenhelm, R.T.E., 2003. Expressions of shallow gas in The Netherlands north sea. Geologie en Mijnbouw/Netherlands Journal of Geosciences 82, 91–105. https://doi.org/10.1017/S0016774600022812.
Seebeck, H., Tenthorey, E., Consoli, C., Nicol, A., 2015. Polygonal faulting and seal integrity in the Bonaparte Basin, Australia. Mar. Petrol. Geol. 60, 120–135. https://doi.org/10.1016/j.marpetgeo.2014.10.012.
Sheriff, R.E., 1975. Factors affecting seismic amplitudes. Geophys. Prospect. 23, 125–138. https://doi.org/10.1111/j.1365-2478.1975.tb00685.x.
Sibson, R.H., 1994. Crustal stress, faulting and fluid flow. Geol. Soc. Spec. Publ. 78, 69–84. https://doi.org/10.1144/GSL.SP.1994.078.01.07.
Smith, A.J., Flemings, P.B., Fulton, P.M., 2014. Hydrocarbon flux from natural deepwater Gulf of Mexico vents. Earth Planet Sci. Lett. 395, 241–253.
Taylor, L., 2012. Noblige-2 (WA-404-P, Carnarvon Basin) Final Well Completion Report.
Taylor, M.H., Dillon, W.P., Pecher, I.A., 2000. Trapping and migration of methane associated with the gas hydrate stability zone at the Blake Ridge Diapir: new insights from seismic data. Mar. Geol.
Tingate, P.R., Khaksar, A., Ruth, P. van, Dewhurst, D., Raven, M., Young, H., Hillis, R., Dodds, K., 2001. Geological controls on overpressure in the northern Carnarvon Basin. The APPEA Journal 41, 573. https://doi.org/10.1071/aj00029.
Traynor, J.J., Sladen, C., 1997. Seepage in Vietnam — onshore and offshore examples. Mar. Petrol. Geol. 14, 345–362. https://doi.org/10.1016/S0264-8172(96)00040-2.
Twartz, S.K., 1981. Well Completion Report Eendracht-1.
van der Aa, D., Allen, P., Ellis, C., Rodger, S., 2013. SATYR 2 Final Well Completion Report Carnarvon Basin. WA-374-P.
van Ruth, P., Hillis, R., Tingate, P., 2004. The origin of overpressure in the Carnarvon Basin, Western Australia: implications for pore pressure prediction. Petrol. Geosci. 10, 247–257. https://doi.org/10.1144/1354-079302-562.

Vejbæk, O.v., Frykman, P., Bech, N., Nielsen, C.M., 2005. The history of hydrocarbon filling of Danish chalk fields. Geological Society, London, Petroleum Geology Conference Series 6, 1331–1345. https://doi.org/10.1144/0061331.

Velayatham, T., 2019. Analysing Ancient Focused Fluid Flow Systems in Offshore Sedimentary Basins of Australia. University of Adelaide.

Velayatham, T., Holford, S.P., Bunch, M., King, R.C., Magee, C., 2019. 3D seismic analysis of ancient subsurface fluid flow in the Exmouth Plateau, offshore western Australia. The Sedimentary Basins of Western Australia V: Proceedings of the Petroleum exploration Society of Australia Symposium 24.

Velayatham, T., Holford, S.P., Bunch, M.A., 2018. Ancient fluid flow recorded by remarkably long, buried pockmark trains observed in 3D seismic data, Exmouth Plateau, Northern Carnarvon Basin. Mar. Petrol. Geol. 95, 303–313. https://doi.org/10.1016/j.marpetgeo.2018.05.007.

Watts, N.L., 1987. Theoretical aspects of cap-rock and fault seals for single- and two-phase hydrocarbon columns. Mar. Petrol. Geol. 4, 274–307. https://doi.org/10.1016/0264-8172(87)90008-0.

Widess, M.B., 1973. How thin is a thin bed? Geophysics 38, 1176–1180.

Winefield, P., Gilham, R., Elsinger, R., 2005. Plumbing the depths of the Central Graben: towards an integrated pressure, fluid and charge model for the Central North Sea HPHT play. Geological Society, London, Petroleum Geology Conference series 6, 1301–1315. https://doi.org/10.1144/0061301.

Young, J.R., 1998. Neogene Nannofossils. Calcareous Nannofossil Biostratigraphy, vol. 225. Kluwer Academic, Dordrecht, p. 265.